Draft version January 10, 2012
Preprint typeset using LaTeX style emulateapj v. 5/2/11

CROSS IDENTIFICATION BETWEEN X-RAY AND OPTICAL CLUSTERS OF GALAXIES IN THE SDSS DR7 FIELD

Lei Wang[1], Xiaohu Yang [1], Wentao Luo[1], Erwin T. Lau[1,2], Yu Wang[3], H.J. Mo[4], Frank C. van den Bosch[5], Q.D. Wang[4]

Draft version January 10, 2012

ABSTRACT

We use the ROSAT all sky survey X-ray cluster catalogs and the optical SDSS DR7 galaxy and group catalogs to cross-identify X-ray clusters with their optical counterparts, resulting in a sample of 201 X-ray clusters in the sky coverage of SDSS DR7. We investigate various correlations between the optical and X-ray properties of these X-ray clusters, and find that the following optical properties are correlated with the X-ray luminosity: the central galaxy luminosity, the central galaxy mass, the characteristic group luminosity ($\propto L_{\rm X}^{0.43}$), the group stellar mass ($\propto L_{\rm X}^{0.46}$), with typical 1-σ scatter of ~ 0.67 in $\log L_{\rm X}$. Using the observed number distribution of X-ray clusters, we obtain an unbiased scaling relation between the X-ray luminosity, the central galaxy stellar mass and the characteristic satellite stellar mass as $\log L_X = -0.26 + 2.90[\log(M_{*,c} + 0.26 M_{\rm sat}) - 12.0]$ (and in terms of luminosities, as $\log L_X = -0.15 + 2.38[\log(L_c + 0.72 L_{\rm sat}) - 12.0]$). We find that the systematic difference between different halo mass estimations, e.g., using the ranking of characteristic group stellar mass or using the X-ray luminosity scaling relation can be used to constrain cosmology. Comparing the properties of groups of similar stellar mass (or optical luminosities) and redshift that are X-ray luminous or under-luminous, we find that X-ray luminous groups have more faint satellite galaxies and higher red fraction in their satellites. The cross-identified X-ray clusters together with their optical properties are provided in Appendix B.

Subject headings: dark matter - X-rays: galaxies: clusters - galaxies: halos - methods: statistical

1. INTRODUCTION

Clusters of galaxies are the most massive virialized objects in the universe. Their abundance and spatial distribution are powerful cosmological probes (e.g., Majumdar & Mohr 2004; Vikhlinin et al. 2009b; Mantz et al. 2010a). In addition, galaxy clusters provide extreme environments for studying the formation and evolution of galaxies within the framework of the hierarchical build-up of the most massive halos. One important property of clusters is that both their stellar and gas components are readily observable: their gravitational wells are deep enough to retain any energetic gas ejected from their member galaxies which can be observed in the optical and infrared. The intracluster medium (ICM) are also hot enough to be observable in X-ray. The observed thermodynamic state of the ICM is determined by the combined effects of shock heating during accretion, radiative cooling, feedback from stellar evolution (stellar winds and supernovae) and active galactic nuclei. The density, temperature, and entropy profiles of the ICM therefore carry important information regarding the entire thermal history of cluster formation. The hot ICM, with temperatures between 10^7K and 10^8K, emits X-rays in the form of thermal bremsstrahlung and atomic line emissions (e.g., Kellogg et al. 1971; Forman et al. 1971). Since the X-ray emission is proportional to the gas density squared, X-ray selected clusters are more suitable than optically-selected clusters for mapping the spatial distribution of clusters as they suffer less from projection effects (Ebeling et al. 1998; Jones & Forman 1999). By assuming hydrostatic equilibrium between the intracluster gas and the cluster potential, one can also derive the gravitational mass of the cluster using density and temperature measurements provided by X-ray data.

Clusters have also been observed by other means in addition to X-ray: optical, infrared, radio, Sunyaev-Zel'dovich effect and gravitational lensing. Among these, the most complete cluster samples to date are optically-selected (e.g. Abell et al. 1989; Zwicky et al. 1961-68) and X-ray selected (e.g. Ebeling et al. 1998; Böhringer et al. 2000). To synthesize the benefits of both X-ray and optical observations of galaxy systems, it is useful to relate the X-ray systems to optically selected groups and clusters. Numerous studies have cross-identified optical groups or clusters with X-ray clusters, or vice versa, in order to compare their optical and X-ray properties (e.g., Bahcall 1977; Edge & Stewart 1991; Donahue et al. 2001, 2002; Yee & Ellingson 2003; Mulchaey et al. 2003; Gilbank et al. 2004). Most of these earlier studies, however, were severely hampered by the lack of large samples with uniform observations in both passbands. The situation improved dramatically with the completion of a number of large surveys. In recent years, with the great advance in optical surveys, especially with the advent of the Sloan Digital Sky Survey (SDSS), more

[1] Key Laboratory for Research in Galaxies and Cosmology, Shanghai Astronomical Observatory, Nandan Road 80, Shanghai 200030, China; E-mail: leiwang@shao.ac.cn
[2] Department of Physics, Yale University, New Haven, CT 06520-8120, USA
[3] Key Laboratory for Research in Galaxies and Cosmology, Center for Astrophysics, University of Science and Technology of China, Hefei, 230026, China
[4] Department of Astronomy, University of Massachusetts, Amherst MA 01003-9305
[5] Department of Astronomy, Yale University, P.O. Box 208101, New Haven, CT 06520-8101, USA

and more effort has been made to characterize the X-ray properties of optically selected clusters (e.g., Mulchaey et al. 2003; Rykoff et al. 2008a,b; Rozo et al. 2009a,b; Hansen et al. 2009; Hao et al. 2010). In particular, Popesso et al. (2004) cross correlated the X-ray clusters from the ROSAT All-Sky Survey (RASS; Voges et al. 1999) with optical data from the SDSS data release 1 (DR1), resulting in a sample of 114 clusters with both X-ray and optical data.

Although X-ray selection is arguably the most reliable method to select clusters, X-ray selection typically has a low efficiency. In fact, a significant fraction of optically detected clusters falls on the general scaling relation between optical luminosity and virial mass (inferred from, for example, the velocity dispersion of the member galaxies), but is undetected in the X-ray (i.e., does not follow the scaling relation between X-ray luminosity and virial mass). This has given rise to the notion that there exists a genuine population of clusters that are X-ray underluminous (e.g., Castander et al. 1994; Lubin et al. 2004; Popesso et al. 2007; Castellano et al. 2011; Balogh et al. 2011). In addition to simply cross-correlating optical and X-ray catalogs, one can also use stacking techniques. Dai, Kochanek & Morgan (2007) used a NIR selected sample of $\sim$ 4000 nearby ($\langle z\rangle \sim 0.02$) galaxy clusters selected from the Two Micron All Sky Survey (2MASS) using a matched filter algorithm (Kochanek et al. 2003), and probed their X-ray properties by stacking X-ray data from the RASS. A similar approach was taken by Rykoff et al. (2008a,b), who used as their input catalog the large maxBCG sample of 14,000 clusters ($\langle z\rangle \simeq 0.23$) selected from the photometric SDSS data (Koester et al. 2007a,b). Although these stacking techniques are extremely powerful for determining the *average* scaling relations between optical and X-ray properties, they contain little to no information regarding the corresponding scatter.

Note that the optical clusters so far are mainly extracted from the photometric data. These photometric samples are quite complete for most massive clusters, (which have the most constraining power as cosmological probes), and they are much deeper than those based on spectroscopic data. However, their galaxy members are not well constrained. In this paper, we use the SDSS DR7 group catalogs of Yang et al. (2007), which are constructed from the SDSS spectroscopic data (Abazajian et al. 2009). These catalogs provide us with galaxy groups that have reliable galaxy memberships which are important in probing the halo occupation distribution (HOD) statistics and galaxy formation models. (e.g. Yang et al. 2008; 2009). The SDSS DR7 group catalogs also span a large halo mass range, from rich clusters to isolated faint galaxies, allowing us to investigate the X-ray luminosity and hot gas distribution not only in massive clusters but also in relatively small halos.

As the first paper in a series, we focus on the cross-identification between the optical galaxy groups with existing X-ray cluster catalogs, e.g. the ROSAT X-ray clusters from the NASA/IPAC Extragalactic Database (NED; see Section 2.2 for their original references). Some straightforward comparisons between the optical and X-ray properties of these clusters are investigated. We will address the more specific probes of the galaxy properties in the X-ray clusters and the X-ray properties around the optical groups in forthcoming papers.

This paper is organized as follows. In Section 2, we briefly describe the group samples of Yang et al. (2007) for SDSS DR7 and our extraction and treatment of the X-ray cluster samples. In section 3, we present the selection criteria for matching groups with X-ray clusters. The correlation between the X-ray and optical properties are investigated in section 4. The properties of groups with and without strong X-ray emissions are compared in Section 5. Finally, we present our conclusions in section 6. Throughout this paper, we use the ΛCDM cosmology whose parameters are consistent with the 7-year data release of the WMAP mission: $\Omega_{\rm m} = 0.275$, $\Omega_\Lambda = 0.725$, $h = 0.702$, and $\sigma_8 = 0.816$, where the reduced Hubble constant, h, is defined through the Hubble constant as $H_0 = 100h$ km s^{-1} Mpc^{-1} (Komatsu et al. 2011).

2. DATA

2.1. *The SDSS DR7 Galaxy and Group catalogs*

The optical data used in our analysis is taken from the SDSS galaxy group catalogs of Yang et al. (2007; hereafter Y07), constructed using the adaptive halo-based group finder of Yang et al. (2005a), here updated to Data Release 7 (DR7). The related galaxy catalog is the New York University Value-Added Galaxy catalog (NYU-VAGC; Blanton et al. 2005b) based on SDSS DR7 (Abazajian et al. 2009), which contains an independent set of significantly improved reductions. DR7 marks the completion of the survey phase known as SDSS-II. It features a spectroscopic sample that is now complete over a large contiguous area of the Northern Galactic cap, closing the gap which was present in previous data releases. From the NYU-VAGC, we select all galaxies in the Main Galaxy Sample with an extinction-corrected apparent magnitude brighter than $r = 17.72$, with redshifts in the range $0.01 \leq z \leq 0.20$ and with a redshift completeness $\mathcal{C}_z > 0.7$. The resulting SDSS galaxy catalog contains a total of 639,359 galaxies, with a sky coverage of 7748 square degrees. Note that a very small fraction of galaxies in this catalog have redshifts taken from the Korea Institute for Advanced Study (KIAS) Value-Added Galaxy Catalog (VAGC) (e.g. Choi et al. 2010)[6].

Following Y07, three group samples are constructed from the corresponding galaxy samples: Sample I, which only uses the 599,301 galaxies with measured r-band magnitudes and redshifts from the SDSS; Sample II, which includes in addition 3269 galaxies with SDSS r-band magnitudes but with redshifts taken from alternative surveys; and Sample III, which includes an additional 36,759 galaxies that do not have redshift measurements due to fiber collisions, but are assigned the redshifts of their nearest neighbors. Although the fiber-collision correction works well in roughly 60 percent of the cases, the assigned redshifts of the remaining 40 percent can be very different from their true values (Zehavi et al. 2002). In this study, in order not to miss any potential group members for cross-identification, we use the group catalogs of Sample III. For completeness, two sets of group catalogs were constructed: one in which we use the Petrosian magnitudes of the galaxies, and the other in which we use the model magnitudes (Yang et al. 2012

[6] These were kindly provided to us by Yun-Young Choi and Changbom Park.

in preparation). In total there are 474,085 groups based on Petrosian magnitudes and 472,673 groups based on model magnitudes. Among these groups about 23,700 have three member galaxies or more. In this paper we use the group catalog based on the model magnitudes. We have tested, though, that using the group catalog based on the Petrosian magnitudes does not affect any of our results in any significant way.

Following Y07, for each group in the catalog, we estimate the corresponding halo mass using the ranking of its characteristic stellar mass, defined as the total stellar mass of all group members with ${}^{0.1}\mathrm{M}_r - 5\log h \leq -19.5$. Here the halo mass function obtained by Tinker et al. (2008) for WMAP7 cosmology and $\Delta = 200$ is used in our calculation, where Δ is the average mass density contrast in the spherical halo. We indicate the group mass thus obtained by $M_{\rm G}$, where the letter 'G' is used to indicate that it has been obtained from the optical group catalog. Note that groups whose member galaxies are all fainter than ${}^{0.1}\mathrm{M}_r - 5\log h = -19.5$ cannot be assigned a halo mass with this method. For these systems, one could in principle use the relation between halo mass and the stellar mass of the central galaxy obtained by Yang et al. (2011) to estimate their halo masses. However, since our main focus is on the cross identification of X-ray clusters with optical groups, which are in general quite massive, we do not require halo masses for these groups.

The halo masses $M_{\rm G}$ thus assigned to the groups are calibrated to correspond to M_{200}, the mass of the halo defined so that it has an average overdensity of 200. Along similar lines, we define the 'virial radius' of the group as r_{200}, which is given by

$$r_{200} = \left[\frac{M_{200}}{\frac{4\pi}{3}\times 200\Omega_{\rm m}\times\frac{3H_0^2}{8\pi G}}\right]^{1/3}(1+z_{\rm G})^{-1}\,, \qquad (1)$$

where $z_{\rm G}$ is the redshift of the group (i.e., the average redshift of the group members). Tests with detailed mock galaxy redshift surveys have shown that the statistical error on $M_{\rm G}$ is of the order of 0.3 dex (see Y07 for details).

2.2. *The X-ray Cluster Catalogs*

The main aim of this paper is to cross-identify the optically selected groups and clusters (described above) with X-ray selected cluster samples and to study the correlations between X-ray and optical properties. For this purpose, we use the ROSAT catalogs at the broad band 0.1-2.4 keV as our primary input sample of X-ray clusters. In particular, we combine the following ROSAT cluster samples: the ROSAT Brightest Cluster Sample (BCS) and their low-flux extensions compiled by Ebeling et al. (1998, 2000), and the Northern ROSAT All-Sky (NORAS) and ROSAT-ESO Flux Limited X-ray (REFLEX) samples compiled by Böhringer et al. (2000, 2004). Within these catalogs, the BCS (Ebeling et al. 1998) has a flux limit $F_X \geq 4.4\times10^{-12}$erg cm^{-2} s^{-1} and flux completeness $f_X \simeq 90$ percent in the northern hemisphere ($\delta \geq 0^\circ$), at high Galactic latitudes ($|b| \geq 20^\circ$). Its low-flux extension (Ebeling et al. 2000) has flux limits $2.8\times10^{-12} \leq F_X \leq 4.4\times10^{-12}$erg cm^{-2} s^{-1} and completeness $f_X \simeq 75$ percent. The NORAS cluster sample (Böhringer et al. 2000) has a flux limit $F_X \sim 1.0\times10^{-12}$erg cm^{-2} s^{-1} and flux completeness $f_X \simeq 50$ percent with respect to REFLEX[7] at $\delta \geq 0^\circ$ and $|b| \geq 20^\circ$. And finally, the REFLEX sample (Böhringer et al. 2004), which covers 4.24 steradians in the southern sky, has flux limits $F_X \geq 3.0\times10^{-12}$erg cm^{-2} s^{-1} and completeness $f_X \geq 90$ percent.

These four catalogs combined contain a total of 1138 unique sources (see the NED website[8]), with information on the rest-frame X-ray luminosity (K-correction applied; e.g. Böhringer et al. 2004) and gas temperature (mostly estimated from the X-ray luminosity) listed for each of the sources. However, 213 entries in this raw, combined X-ray cluster sample are duplicates, implying a total sample of 925 unique sources, many of which have already been cross-identified with Abell or Zwicky clusters in NED. For duplicate clusters, we take the ones with the most up-to-date information for their characteristic quantities. Throughout, we use $L_{\rm X}$, $T_{\rm X}$, $M_{\rm X}$, $R_{\rm X}$, to denote the X-ray luminosity, gas temperature, halo mass and halo radius for each X-ray cluster, where $M_{\rm X}$ and $R_{\rm X}$ are defined later in Eq. 3. These quantities are quoted in units of 10^{44}erg s^{-1}, keV, $h^{-1}\mathrm{M}_\odot$ and h^{-1}Mpc, respectively.

As a first step of our cross identification we remove those X-ray clusters that are located outside the sky area and redshift range covered by the SDSS DR7. For each X-ray cluster we adopt the right ascension, declination, and redshift, z, recommended by the NED website, unless the information provided by NED is incomplete, in which case we use the data from the most recent documentation. Only clusters with $0.01 \leq z \leq 0.20$ and with a SDSS redshift completeness of $\mathcal{C}_z > 0.7$ at the cluster's center are kept. This results in a sample of 217 unique X-ray clusters. As a final selection criterion, we follow Y07 and remove all X-ray clusters that suffer significantly from an edge effect (i.e., are located close to one or more boundaries of the SDSS survey volume), which leaves a sample of 207 unique sources.

Throughout this paper, if not specified otherwise, we use the subscripts 'g', 'G' and 'X' to refer to quantities for galaxies, optical groups and X-ray clusters, respectively.

3. MATCHING OPTICAL GROUPS WITH X-RAY CLUSTERS VIA CENTRAL GALAXIES

Since we have only 207 X-ray clusters, we decide to use simple eyeball checks to make the cross-identification with optical groups. Our criterion to cross-identify X-ray clusters with optical groups is based on their common central galaxies.

To find the central galaxies for our sample of 207 X-ray clusters, we make use of the SDSS skyserver to extract an optical image around each X-ray cluster. In each of these images we first find the brightest galaxy according to its apparent r-band magnitude provided by the skyserver within a 7 arcmin radius from the center of the X-ray cluster [9]. If this galaxy is red [with ${}^{0.1}(g-r) > 0.8$]

[7] Note that this value is estimated in the $9^{\rm h} - 14^{\rm h}$ region.

[8] http://nedwww.ipac.caltech.edu/

[9] Since different X-ray source characterization techniques were used by Ebeling et al. (1996, 1998, 2000; Voronoi tessellation and percolation, VTP) and Böhringer et al. (2000, 2004; Growth curve analysis, GCA), the position difference from different references can be as large as ~ 5 arcmins for a given source

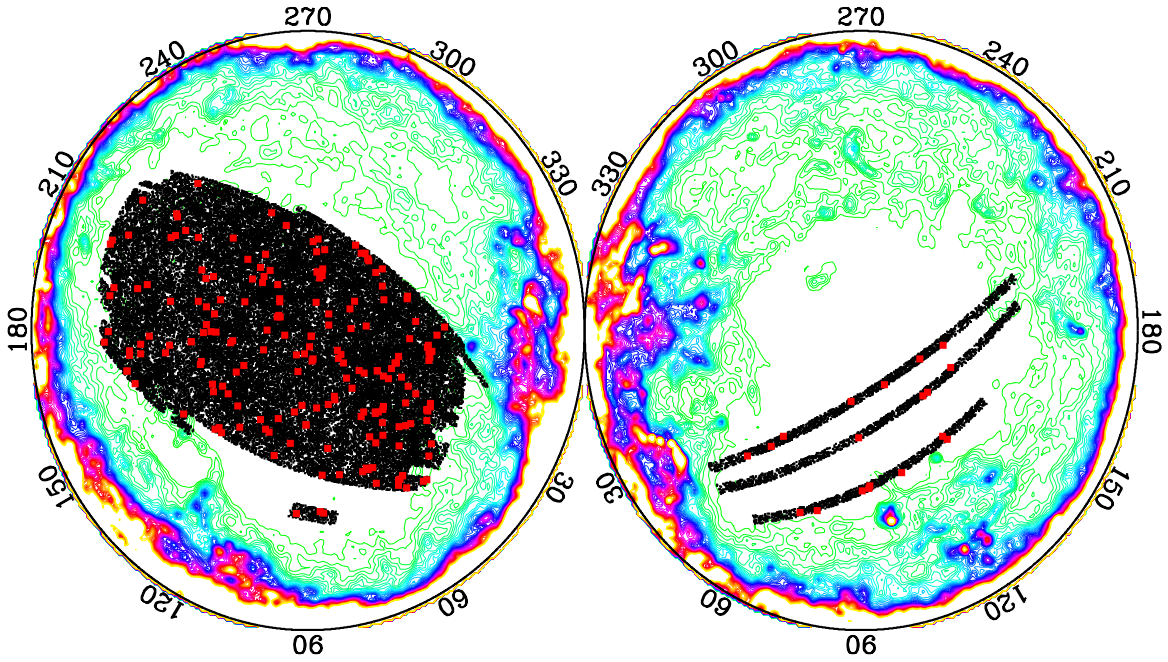

FIG. 1.— The distribution of X-ray clusters (squares) that coincide with the sky coverage of the SDSS DR7 galaxies (black area), overlaid on the galactic extinction contours of Schlegel, Finkbeiner & Davis (1998).

and has an offset smaller than 2 arcmins from the X-ray cluster position obtained from Ebeling et al. (1998, 2000) and Böhringer et al. (2000, 2004), it is regarded as the central galaxy of the cluster. This criterion follows that of Allen et al. (1992) and Crawford et al. (1995, 1999) who showed that the bright central galaxy is usually found within 1-2 arcmin of the centroid of the X-ray emission of the cluster. About 170 clusters in our final catalogue are found in this catagory. For all the other X-ray clusters, where the brightest galaxies have offsets $\gtrsim$ 2 arcmins from the ROSAT X-ray cluster positions, we make use of high-resolution X-ray images from e.g. ROSAT/PSPC, ROSAT/HRI, XMM-Newton and Chandra when available, or from previous identifications (e.g. Crawford et al. 1995, 1999). About 20 central galaxies are identified with the high-resolution X-ray images, and the remaining $\sim$ 10 are based on previous identifications (see the notes on individual sources in Table 1). An exception is RXC J1554.2 +3237 for which no bright and red galaxy is found within 10 arcmins from the X-ray cluster center. This cluster is therefore removed from our sample. Close inspection shows that large offsets mainly come from (i) multiple maxima in the X-ray images, e.g. the X-ray cluster position is located between the 2 maxima of the X-ray emission; (ii) very extended sources for which the uncertainty in the position of the X-ray maximum is very large; and (iii) low resolution of RASS for which the 2 pixel offset along pixel's diagonal line is larger than 2 arcmins.

As a further check of the reliability of our central galaxy identification, we overlay the X-ray contour of each cluster on the optical image. We find that the central galaxy is in general located close to the X-ray flux maximum. In fact, for each of the 90 clusters where high-resolution (with pixel sizes about one arcsecond and position error about a few arcseconds) X-ray data are available from the Chandra and/or XMM-Newton databases, we find that the peak of the X-ray emission is almost exactly ($\leq$ 5 arcsec) centered on the 'central galaxy' that we have identified using the method described above. In summary, among all the X-ray clusters that are identified with central galaxies, about 170 have $<$ 2 arcmin offsets from the X-ray cluster positions, about 30 have $>$ 2 arcmin offsets, and only 2 have offsets larger than 7 acrmins. For the last two cases, the X-ray distributions are very extended. The offsets between the central galaxies and the X-ray cluster positions are provided in Appendix B.

Although NED provides redshifts for all X-ray clusters in our sample, these are not always reliable. For example, for clusters for which no spectroscopic redshift information is available, Ebeling et al. (1996; 1998; 2000) assign a redshift to the X-ray cluster based on the magnitude of the tenth brightest galaxy (cf., Abell 1958; Corwin 1974; Abell et al. 1989; Peacock & West 1992). Since each of the X-ray clusters in our sample is linked to a central galaxy, we can use the spectroscopic SDSS galaxy catalog to obtain improved redshifts for these X-ray clusters. Unfortunately, because of fiber collisions, which are relatively frequent for galaxies in high-density regions such as clusters, spectroscopic redshifts are only available for $\sim$ 75 percent of the central galaxies in our sample of X-ray clusters. For the remaining $\sim$ 25 percent the redshifts are obtained using the redshifts of the nearest (or the second, third, ..., nearest) galaxies close to the central galaxies[10]. Both the original and updated redshift for

[10] For these central galaxies without spectroscopic redshifts, the redshifts provided in the NYU-VAGC according to the nearest neighbors may not be always correct. Since we have made eyeball check of each 'central' galaxy with respect to its neighboring

each X-ray cluster are provided in Appendix B. For the updated one we indicated whether it corresponds to the spectroscopic redshift of the central galaxy (ztype= 1) or whether it has been estimated from the neighboring galaxies (ztype= 2). In 204 of the 206 cases the updated redshift agrees with the original redshift to better than $\Delta z = 0.02$. Throughout this paper we use our updated redshifts, and all related quantities, such as $L_{\rm X}$, $M_{\rm X}$, and $R_{\rm X}$ have been updated accordingly.

Starting from the central galaxies associated with the X-ray clusters, we look into the SDSS DR7 group catalog for the cross-identified galaxy groups. We find that not all the central galaxies in the X-ray clusters are the most massive galaxies (MMG) in their respective groups. About 20 (10%) of the X-ray clusters have galaxies more massive than the centrals and which are offset from the X-ray center by more than 7 arcmins. This is in agreement with other studies; for example, Zhang et al. (2011), using 62 galaxy clusters in the HIghest X-ray FLUx Galaxy Cluster Sample (HIFLUGCS; Reiprich & Böhringer 2002), have shown that the brightest galaxy in the cluster has a lognormal offset from the X-ray flux-weighted center with a mean value of about 10kpc and a 10-based logarithmic scatter of 0.55 (see also Skibba et al. 2011 and references therein). In what follows, we will use subscripts 1 and c to refer to the most massive galaxies and the central galaxies, respectively (e.g., in case of the luminosities we will use L_1 and L_c).

As a final step of our cross-identification, we check for duplicates (clusters that are cross-identified with the same central galaxy) and pairs of merging clusters (clusters that are cross-identified with the same optical group, but with different central galaxies), as outlined in Appendix A. In both cases we remove the smaller of the two clusters from our sample. This results in a final sample of 201 X-ray clusters with an optical cross-identification in our SDSS DR7 group catalog. As an illustration, Fig. 1 shows the distribution of these X-ray clusters on the sky overlaid on the distribution of galaxies in the SDSS DR7. Before we proceed with studying the correlations of their X-ray and optical properties, we point out that many of the rich optical clusters/groups in our group catalog are not associated with any existing X-ray cluster entries. We will address this issue in detail in Section 5.

4. CORRELATION BETWEEN THE X-RAY AND OPTICAL PROPERTIES

Now that we have cross-identified the X-ray clusters with optical groups, we proceed by examining various (possible) correlations between the X-ray and optical properties of the X-ray clusters.

4.1. *The General Correlations*

The optical properties to be investigated in this subsection include the characteristic luminosity L_G and stellar mass $M_{\rm st}$ of the group/cluster, defined as the total luminosity and total stellar mass of all member galaxies with ${}^{0.1}{\rm M}_r - 5\log h \leq -19.5$, respectively (see Y07 for more detail). In addition, we will also consider the following properties of their central galaxies: the r-band luminosity L_c, the stellar mass $M_{*,c}$, the ${}^{0.1}(g-r)$ color, and the concentration index $c = r_{90}/r_{50}$[11]. We examine if there are any correlations between these properties and the X-ray cluster luminosity $L_{\rm X}$.

We first examine the distributions, as a function of X-ray cluster luminosity, of the stellar mass and luminosity of the central galaxies. The results are shown in the upper row panels of Fig. 2: left panel is for the stellar mass and right panel for the luminosity. There are clear correlations between these quantities. To quantify these correlations, we use a least square linear regression method in the log-space to obtain the regression lines. Here we did not take into account measurement errors in $L_{\rm X}$ and $M_{*,c}$ (or L_c) as they are much smaller than the scatter among different clusters. The same weight is assigned to each cluster in the fitting. The best-fit lines are shown as the solid lines, together with their parameters, in the corresponding panels. For both relations the correlation coefficient is about 0.63. As an illustration, we also show as the short-dashed lines the $\pm1\sigma$ scatter of the distributions with respect to the best fit lines. For fixed L_X, the 1σ scatter is ~ 0.20 dex and ~ 0.18 dex in $M_{*,c}$ and L_c, respectively. For fixed $M_{*,c}$ (L_c), the scatter in L_X is $\sim 0.20/0.30 = 0.67$ dex ($0.18/0.27 = 0.67$ dex). Despite the relatively large scatter, there is a clear trend that clusters with brighter X-ray luminosities have central galaxies that are more massive and more luminous. The correlation slope between the stellar mass (luminosity) of the central galaxies and the cluster X-ray luminosity is ~ 3.5. However, since the X-ray cluster sample is flux limited, the correlations may be affected by the Malmquist bias. We will come back to this issue in Section 5.1.

Next we check the distributions of the ${}^{0.1}(g-r)$ color and the concentration index, c, of the central galaxies, again as a function of X-ray cluster luminosity. The distributions are shown in the lower panels of Fig. 2. Clearly, the majority of central galaxies in X-ray clusters are red and of early-type (relatively large concentration parameters). Here, we did not see any obvious correlation between the color (or concentration) and the X-ray luminosity of the cluster.

Apart from those properties of central galaxies, we proceed to investigate the properties of groups. We show in the upper panels of Fig. 3 the distributions of the characteristic stellar mass ($M_{\rm st}$; upper left-hand panel) and the characteristic luminosity ($L_{\rm G}$; upper right-hand panel) as a function of $L_{\rm X}$. Similar to the case of the central galaxy, we see a clear positive correlation between the group stellar mass (luminosity) and its X-ray luminosity. Using the same algorithm for central galaxies, we fit the regression lines for the groups. The results are shown in the upper panels of Fig. 3 as solid lines. The slopes of the best-fit lines are somewhat smaller (~ 2.5) than in the case of the stellar mass/luminosity of the *central* galaxy. Here again, we show using the short-dashed lines the $\pm1\sigma$ statistical scatter of the distributions with respect to the best fit lines. The 1σ scatters are about 0.29dex in $M_{\rm st}$ and L_G for a given L_X, or $0.29/0.46 = 0.63$dex

galaxies, if its nearest neighbor is an isolated blue galaxy, we suspect this galaxy has been assigned a wrong redshift. In that case we update its redshift with that of the second (or third, etc.) nearest galaxy with red colors, and with a few more galaxies at the same redshift, i.e. the most possible redshift for the cluster.

[11] r_{50} and r_{90} are the radii containing 50% and 90% of the Petrosian flux (Blanton et al. 2005), respectively.

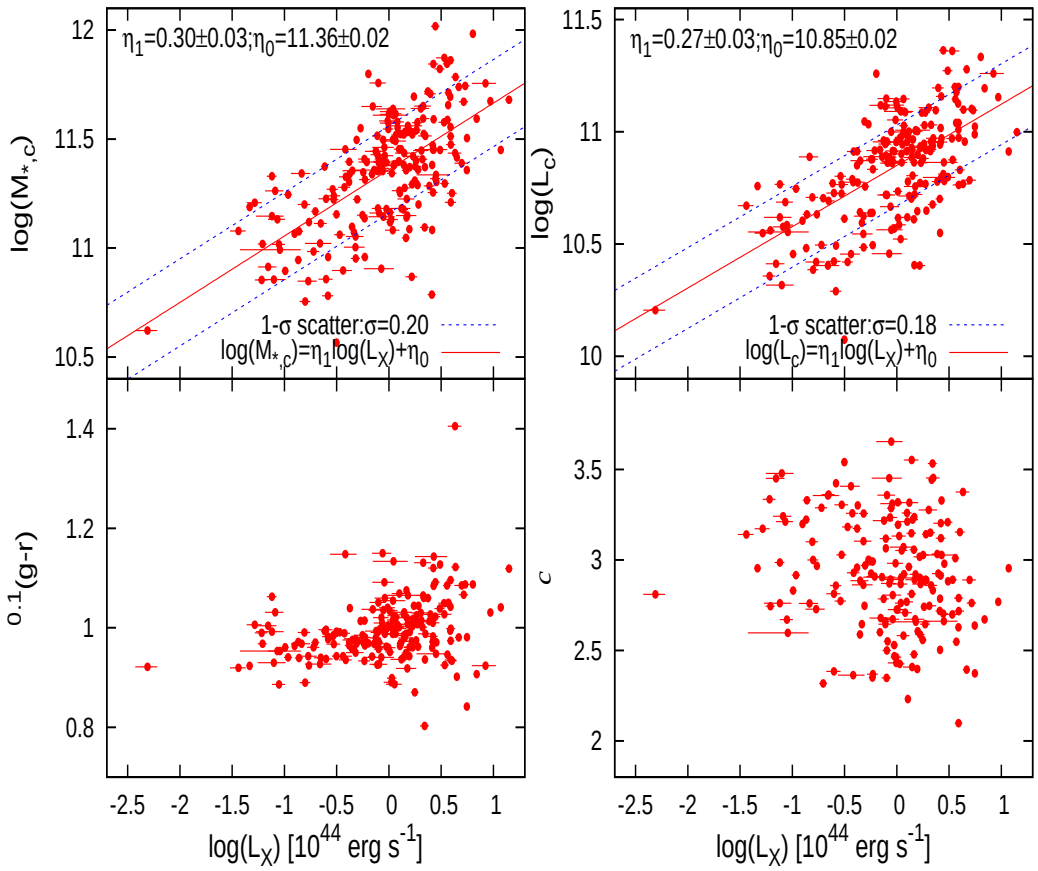

FIG. 2.— The distributions of various optical properties of central galaxies as a function of the X-ray luminosity of their host cluster, $L_{\rm X}$. Clockwise from the upper left-hand panel, the optical properties of the central galaxies are the stellar mass, $M_{*,c}$, the luminosity, L_c, the $^{0.1}(g-r)$ color, and the concentration parameter c. The solid and dashed lines in the upper two panels are the best fit and 1-σ deviations of the $M_{*,c}-L_{\rm X}$ and $L_c-L_{\rm X}$ relations, respectively.

and $0.29/0.43 = 0.67$dex in L_X for a fixed $M_{\rm st}$ and $L_{\rm G}$. And we will also check if these relations are significantly affected by the Malmquist bias in Section 5.1.

Finally, we check the distributions of the stellar mass and luminosity gaps between the first and second most massive (luminous) galaxies. The results are shown in the lower-left and lower-right panels in the middle row of Fig. 3, respectively. As discussed in D'Onghia et al. (2005) and Milosavljević et al. (2006) this gap statistic quantifies the dynamical age of a system of galaxies: haloes with a small gap must be relatively young, as dynamical friction will cause multiple luminous galaxies in the same halo to merge on a relatively short time scale. Evidently, there is no obvious correlation between the stellar mass gap or luminosity gap and the cluster's X-ray luminosity. Furthermore, a comparison with the distributions of the luminosity and stellar mass gaps in massive groups presented in Yang et al. (2008), shows that the X-ray clusters have gaps that are in excellent agreement with those expected for haloes with $M_h \gtrsim 10^{14}\,h^{-1}{\rm M}_\odot$ (see also van den Bosch et al. 2007). Hence, there is no indication that the magnitude of the luminosity and/or stellar mass gaps are in any way correlated with X-ray luminosity.

In the literature, the luminosity gap has often been used to define a "special population" of galaxy groups, called "fossil groups", which are defined as having an R-band luminosity gap $\log L_1 - \log L_2 > 0.8$ (e.g. Ponman et al. 1994). These fossil groups are usually dominated by one central early-type galaxy, and a bright extended X-ray halo with a cooling time that is long enough for its bright satellite galaxies to have merged away (i.e., to have been cannibalized or disrupted by the central galaxy). Among our 201 X-ray clusters, only 2 fall in this category (the clusters with the sequence numbers 46 and 73 in Appendix B). In addition, there are 3 clusters in our sample that have no satellite galaxies above the apparent magnitude limit $r = 17.72$ (not observed since $L_2 < L_{\rm limit}$), which might be fossil groups as well. Their gaps are plotted as lower limits (upward pointing arrows) using $L_2 = L_{\rm limit}$. Note that all five potential fossil groups in our sample have relatively high X-ray luminosities, suggesting either (i) that they reside in relatively massive haloes, or (ii) that their X-ray luminosity is a poor indicator of their halo mass. Unfortunately the sample is too small to draw any meaningful conclusions. Nevertheless, as the X-ray clusters are of quite different gap distributions, we will check in more detail the galaxy properties (e.g., the star formation rate, etc.) in X-ray clusters within different gap regions in a future probe.

4.2. *The Halo Masses of the X-ray Clusters*

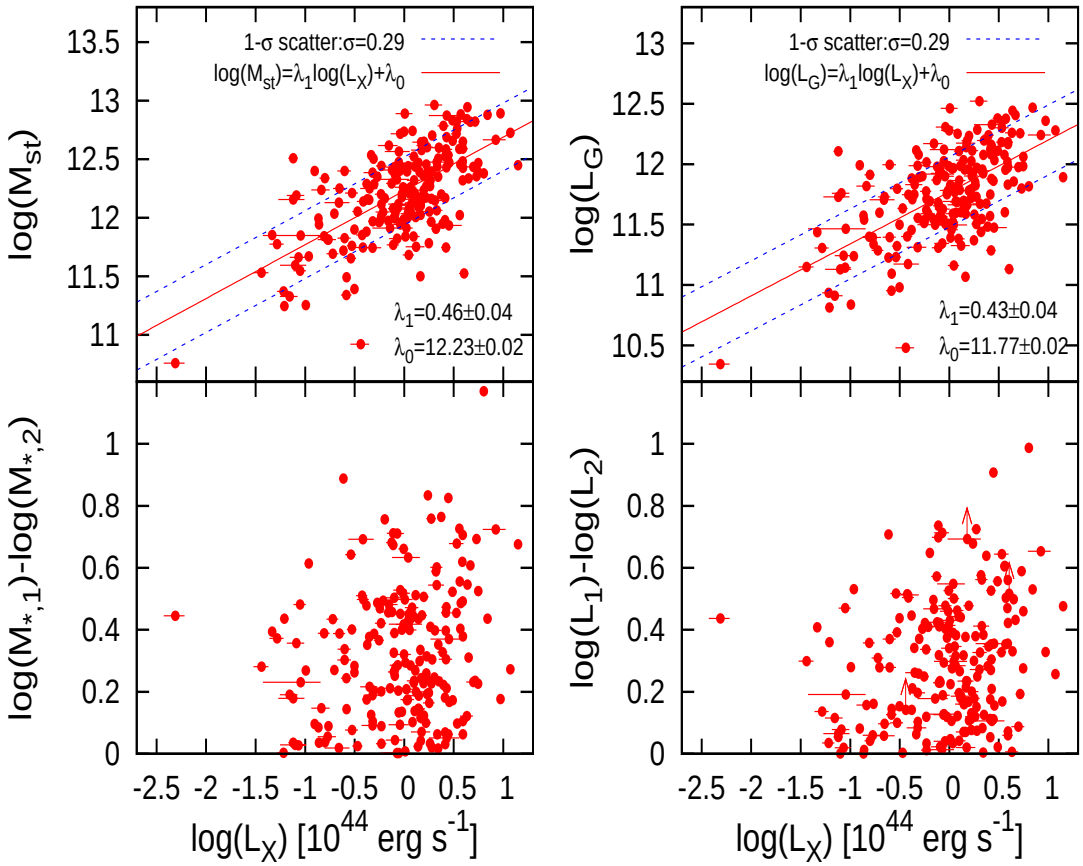

FIG. 3.— Upper panels: the distributions of characteristic stellar masses (left) and luminosities (right) of groups as a function of X-ray cluster luminosity $\log L_{\rm X}$. Lower panels: the distributions of stellar mass gaps between the first and second most massive galaxies (left) and the luminosity gaps between the first and second brightest galaxies (right) as a function of $\log L_{\rm X}$. The solid and dashed lines in the upper row panels are the best fit and 1-σ deviations of the $M_{\rm st} - L_{\rm X}$ and $L_G - L_{\rm X}$ relations, respectively.

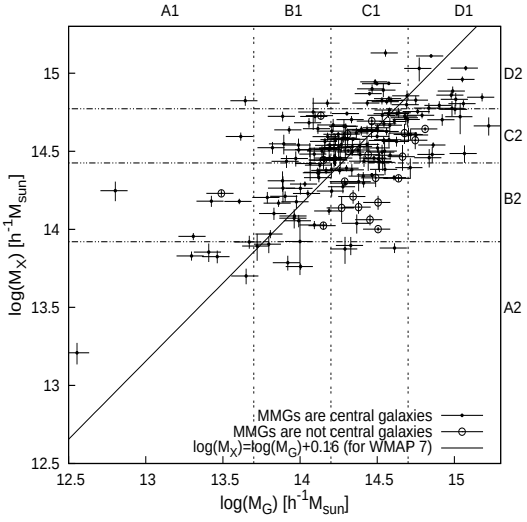

FIG. 4.— The X-ray cluster mass $\log M_{\rm X}$ v.s. the cross identified group mass, $\log M_{\rm G}$. Here results are shown for X-ray clusters in which the most massive galaxies are (solid symbols) or are not (open symbols) central galaxies. To check their large scale environments, the X-ray clusters are divided into 4 subsamples (A1-D1) according to $\log M_{\rm G}$ using the three vertical dashed lines shown in the plot. For comparison, we also divide the X-ray clusters into 4 subsamples (A2-D2) according to $\log M_{\rm X}$, each containing exactly the same number as the corresponding subsample in A1-D1.

In this section we compare two different methods to estimate the halo masses of the X-ray clusters in our sample. The first method is the one presented and tested in Y07, and uses abundance matching to infer a halo mass for each group in the SDSS group catalog, under the assumption of a one-to-one (i.e., zero scatter) relation between halo mass and either $L_{\rm G}$ or $M_{\rm st}$. As shown in Yang et al. (2005a) and Y07, the typical uncertainty in the resulting halo mass (hereafter M_G) is at the level of $\sigma_{\log M_G} \sim 0.3$. However, since the majority of the groups contain only one or two members, if we restrict to groups with at least 3 members[12], the resulting uncertainty is about $\sigma_{\log M_G} \sim 0.25$. The second method that we consider in this section is the hydrodynamical mass, M_X, inferred from the X-ray emission under the assumption that the cluster is in hydrostatic equilibrium. In what follows we convert all halo masses to the same definition, namely the mass inside a spherical volume of radius r_{200}, inside of which the average density is 200 times the background density of the Universe. By construction, the masses M_G are already consistent with this definition.

The hydrodynamical mass, M_X, requires accurate measurements of the radial temperature profile of the

[12] Among 201 groups that are matched with the X-ray clusters, 197 have at least 3 members.

ICM. Since such data is only available for a tiny fraction of the 201 X-ray clusters in our sample, we use a statistical method instead, based on the *average* $L_{\rm X}-M_X$ relation (e.g. Reiprich & Böhringer 2002; Stanek et al. 2006; Vikhlinin et al. 2009; Leauthaud et al. 2010; Arnaud et al. 2010) . Since we focus only on low-redshift ($0.01\leq z\leq 0.2$) X-ray clusters, with rest-frame X-ray luminosities measured in the broad ROSAT passband (0.1-2.4 keV), we use the $L_{\rm X}$-M_X relation of Arnaud et al. (2010). By investigating the regularity of cluster pressure profiles with REXCESS (Böhringer et al. 2007) for a representative sample of 33 local ($z<0.2$) clusters, and with the help of N-body/hydrodynamical simulations, Arnaud et al. (2010) obtained the following X-ray luminosity-mass scaling relation,

$$\frac{L_{\rm 500c}}{10^{44}{\rm erg\ s^{-1}}}=C\Big(\frac{M_{\rm 500c}}{3\times10^{14}M_\odot}\Big)^{\alpha}\left[\Omega_{\rm m}(1+z)^3+\Omega_\Lambda\right]^{\frac{7}{6}}\,, \tag{2}$$

where $\log(C)=0.193$, and $\alpha=1.76$. $M_{\rm 500c}$ is the halo mass of the X-ray cluster within radius $r_{\rm 500c}$ whose average mass density is 500 times the critical mass density of the Universe, and $L_{\rm 500c}$ is the total X-ray luminosity within $r_{\rm 500c}$. This fitting formula has an intrinsic scatter in the log-log plane of $\sigma_{\log M_{\rm 500c}}=0.199$. Note that the X-ray luminosity $L_{\rm X}$ used in this paper is the total luminosity without cluster core exclusion. Piffaretti et al. (2010) employed an iterative algorithm to calculate $L_{\rm 500c}$ for sources with available aperture luminosities $L_{\rm ap}$, and found $L_{\rm 500c}/L_{\rm X}=0.91$ for the total X-ray luminosities. With this transformation, we can obtain $M_{\rm 500c}$ and $r_{\rm 500c}$ for an X-ray cluster with given $L_{\rm X}$. The final step is then to convert $M_{\rm 500c}$ to M_{200}, for which we use the relations

$$\begin{aligned} r_{200}&\simeq 2.70\times r_{\rm 500c}\,,\\ M_{200}&=M_{\rm 500c}\times\frac{200}{500}\times\Omega_{\rm m}\times\left(\frac{r_{200}}{r_{\rm 500c}}\right)^3\,, \end{aligned} \tag{3}$$

where we have assumed that dark matter have a NFW density profile (Navarro et al. 1997) with concentration parameters given by the concentration-mass relation of Maccio et al. (2007). Note that we have not made a distinction between cool-core and non cool-core systems. As shown in Pratt et al. (2009), the L_X-M_X relation for cool-core clusters has a systematically higher normalization than non cool-core systems. We will come back to this in a forthcoming paper by probing the optical properties of galaxies in cool-core and non cool-core systems.

Fig. 4 plots the hydrodynamic mass M_X versus the group mass M_G. There is a clear correlation between these two sets of halo masses, with a lognormal scatter at the level of $\sigma_{\log M_{\rm X}}\sim 0.25$. This is perhaps due to mixing of cool-core and non cool-core clusters in the sample. For comparison, results are shown separately for X-ray clusters for which the most massive galaxies are (solid dots) and are not (open circles) central galaxies. There is a hint that X-ray clusters with none central MMGs are slightly more massive in terms of group mass M_G.

To check if there is any systematic difference between these two sets of halo mass measurements, we again fit using the least square linear regression method with only 1 free parameter, $\Delta\log M$ to obtain the best fit $\log M_X=\Delta\log M+\log M_G$ relation. The result is shown in Fig. 4 as the solid line. Here we see small but noticeable systematic difference between the two sets of halo masses. Note that the halo masses obtained in Y07 are based on the abundance matching method where the halo mass function of given cosmology (WMAP7 in this paper) is used. Thus obtained halo masses are quite sensitive to the cosmological parameters. In case the M_X provided by the X-ray scaling relation is reliable, the systematic difference can be straightforwardly used to probe the cosmology. For instance, here the slightly underestimated systematic difference for M_G may indicate that the data require the slightly larger Ω_m and/or σ_8 than WMAP7. And of cause, to carry out reliable constraints along this line, more detailed error analyses are needed.

4.3. *Distribution of Galaxies inside and around X-ray Clusters*

As a general check of the X-ray cluster masses $M_{\rm G}$ and M_X, we make use of the fact that, in CDM cosmologies, more massive haloes are more strongly clustered (e.g., Mo & White 1996). Hence, if our mass indicators are reliable, we should find that haloes with larger M_X or M_G are located in denser environments. We can check this using the distribution of galaxies in the cluster outskirts. To do so, we proceed as follows. We first divide our sample of 201 X-ray clusters in four subsamples (A1-D1) according to their assigned mass M_G, and in another set of four subsamples (A2-D2) according to their assigned mass M_X. The samples are indicated in Fig. 4 as horizontal and vertical dot-dashed lines.

Since the typical velocity dispersion of cluster galaxies is $\sim 1000\,{\rm km\,s^{-1}}$, we measure the surface number density of galaxies in and around X-ray clusters as a function of the projected distance

$$r_{\rm p}=\sqrt{|\mathbf{r}_{\rm X}-\mathbf{r}_{\rm g}|^2-(d_{\rm X}-d_{\rm g})^2}\,, \tag{4}$$

using the following criterion:

$$c\Delta z=c|z_{\rm X}-z_{\rm g}|\leq 1000\,{\rm km\,s^{-1}}\,. \tag{5}$$

Here c is the speed of light, while ($z_{\rm g}$, $\mathbf{r}_{\rm g}$, $d_{\rm g}$) and ($z_{\rm X}$, $\mathbf{r}_{\rm X}$,$d_{\rm X}$) are the redshifts, co-moving coordinates, and co-moving radial distances from the observer, of the galaxy and the X-ray cluster (i.e., its central galaxy) in question. To avoid potential inhomogeneities caused by Malmquist bias, we use a volume-limited galaxy sample with ${}^{0.1}{\rm M}_r-5\log h\leq -21.27$.

Fig. 5 shows the resulting galaxy surface number densities, $\Sigma_{\rm gal}(r_{\rm p})$ for the X-ray clusters in the four subsamples (A1-D1) of mass M_G (left-hand panel) and the four subsamples (A2-D2) of mass M_X (right-hand panel). In each panel the vertical arrow indicates the average halo radius, r_{200}, of the X-ray clusters in consideration. On small scales ($r_{\rm p}\lesssim r_{200}$), the signal is dominated by galaxies that reside in the dark matter halo of the cluster. To show this we determine the '1-halo' term by simply computing the average projected surface number density of all galaxies that belong to the X-ray clusters in each bin *according to the Y07 group catalog*. These are shown as the dotted histograms in Fig. 5, and, as expected, nicely overlap with $\Sigma_{\rm gal}(r_{\rm p})$ on small scales. Note that in the two most massive bins (D1 and D2) these 1-halo terms are somewhat larger than $\Sigma_{\rm gal}(r_{\rm p})$, which is a result of

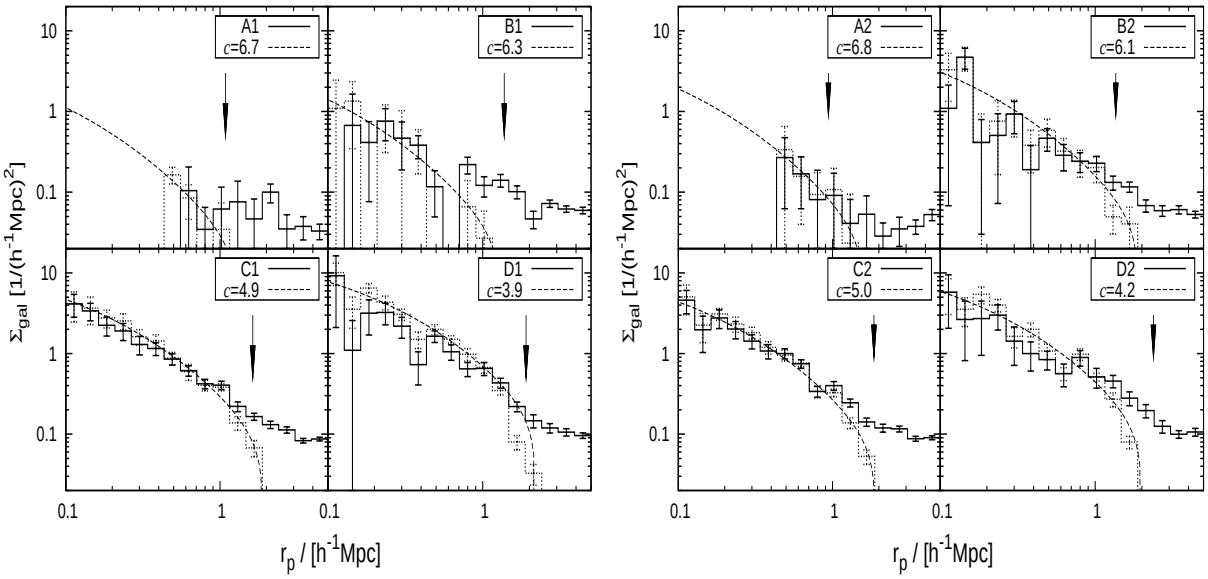

FIG. 5.— Surface number density of galaxies in and around X-ray clusters in units of $1/(\,h^{-1}\mathrm{Mpc})^2$. Different panels correspond to different X-ray cluster subsamples. The error bars are 1σ scatter obtained from 200 bootstrap re-samplings. The vertical arrow in each panel indicates the average halo radius, r_{200}, of the X-ray clusters in consideration. The dashed lines are the best fit 2-D NFW profiles.

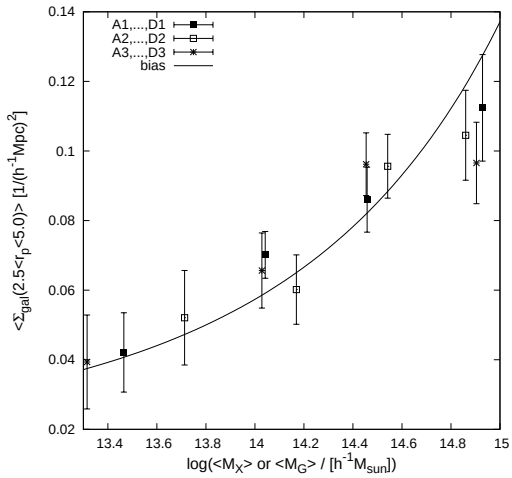

FIG. 6.— The average galaxy surface number density within $2.5\,h^{-1}\mathrm{Mpc} < r_\mathrm{p} < 5\,h^{-1}\mathrm{Mpc}$ as a function of halo mass M_X or M_G. The errorbars are obtained from 200 bootstrap re-samplings of the clusters/groups in consideration. For comparison, we show as the solid line the halo bias predicted by Sheth et al. (2001), properly shifted to match most of the data points.

our cut in redshift space (criterion [5]). We fit the 1-halo term profiles with a projected NFW model (Eq. 7 in Yang et al. 2005a), and the results are also plotted in Fig. 5 as the dashed curves. The concentration parameters c thus obtained are indicated in each panel. Compared to theoretical predictions for the concentration parameters of dark matter haloes (e.g., Zhao et al. 2009), these best fit concentrations c are somewhat lower, suggesting that satellite galaxies have a number density distribution that is less centrally concentrated than the dark matter. Although in qualitative agreement with other studies (e.g., Lin et al. 2004; Collister & Lahav 2005; Yang et al. 2005b; Chen 2008; More et al. 2009), we caution that, because of interlopers and other selection effects, a more quantitative measure of the true concentration of the number density distribution of satellite galaxies requires a more careful analysis (e.g. Yang et al. 2005b; Chen 2008).

At large projected radii ($r_\mathrm{p} \gtrsim r_{200}$) the galaxy surface number densities, $\Sigma_\mathrm{gal}(r_\mathrm{p})$, flatten over to roughly constant values. A comparison with the 1-halo terms shows that this reflects the distribution of galaxies in the direct surroundings of the clusters. Since all surface number density profiles are obtained using the same volume limited sample of galaxies, the ratios between the large-scale surface number densities are directly proportional to the ratios of the biases of the X-ray clusters in the different subsamples. We show in Fig. 6 the average galaxy surface number densities within $2.5h^{-1}\mathrm{Mpc} < r_\mathrm{p} < 5h^{-1}\mathrm{Mpc}$ as a function of halo mass, M_G (solid squares) or M_X (open squares). Clearly, more massive clusters have higher galaxy surface number density, indicating that they reside in denser environments (i.e., are more strongly biased). For comparison, the solid line in Fig. 6 is the halo bias predicted by Sheth et al. (2001), properly shifted in the vertical direction to match most of the data points. Clearly, the data and model prediction agree remarkably well, for both M_G and M_X.

5. GROUPS WITH AND WITHOUT STRONG X-RAY EMISSION

Having discussed various optical and X-ray correlations for the groups that are linked with X-ray clusters, we now focus on groups of comparable masses (M_G) but lacking strong X-ray emission (i.e., for which no measurement of L_X is available). Although both samples have the same sky coverage and lie in the same redshift range, many groups fall in this category even the richest ones. There are of cause various survey selections, e.g. in the X-ray fluxes, in the bright star mask, etc., that prevent us from getting a complete X-ray cluster catalogue. The number is much larger than those completeness values quoted in e.g. Ebeling et al. (2000).

In this section, we investigate the possible Malmquist

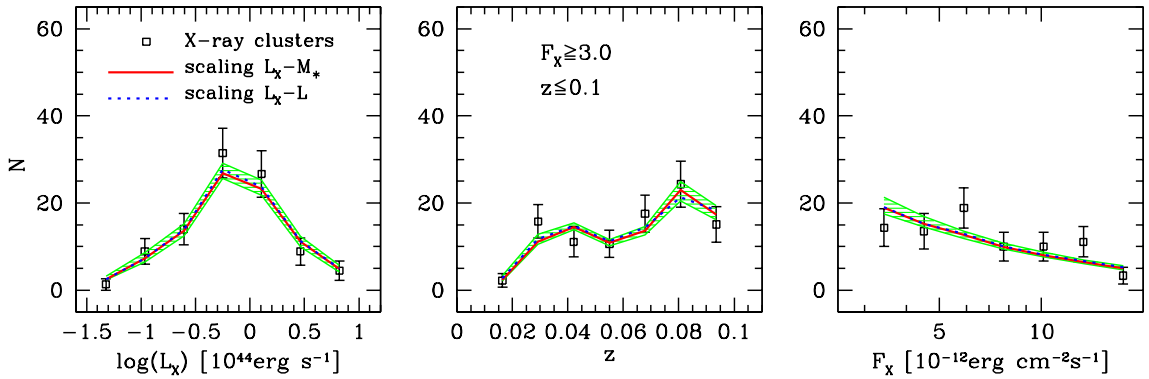

FIG. 7.— The differential number distribution of X-ray clusters in the SDSS DR7 region with $F_X \geq 3.0 \times 10^{-12}$ erg cm^{-2} s^{-1} and redshift $z \leq 0.1$ (squares with error bars) as a function of X-ray luminosity (left panel), redshift (middle panel) and X-ray flux (right panel), respectively. The solid and dashed lines in each panel are the best fit model predictions by the scaling relations using group stellar masses and luminosities, respectively. The shaded areas represent the 68% ranges of the model predictions.

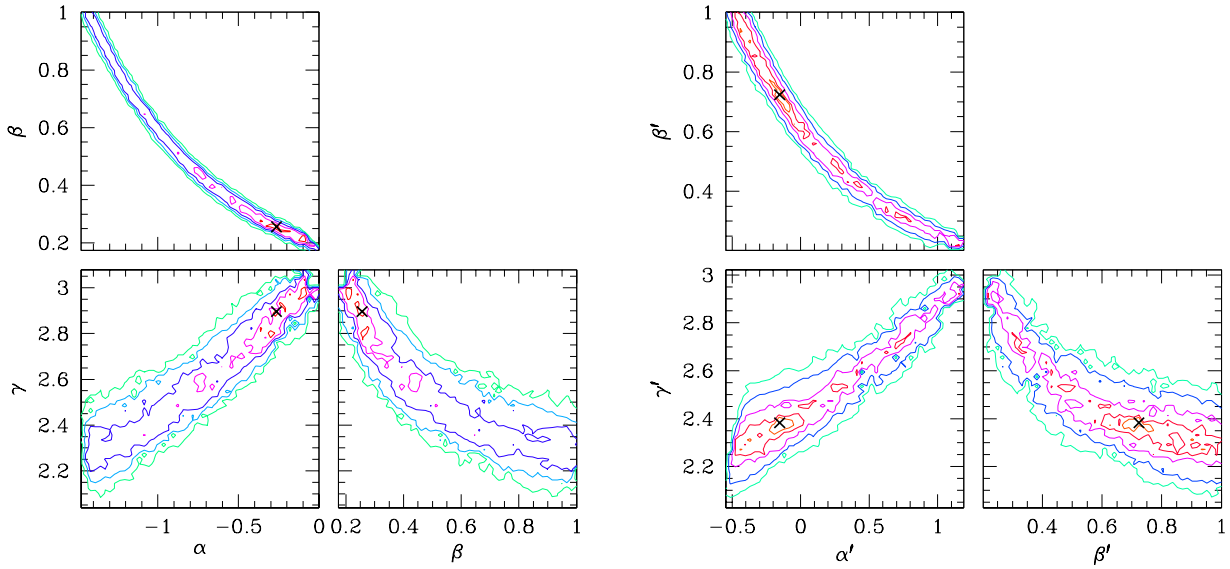

FIG. 8.— The best fit (cross) and the projected distribution of the parameters on 2-D planes. The outer first and second contours correspond to the distribution of the 95% and 68% parameters starting from the smallest χ^2 values. Here results shown in the left and right panels are for stellar mass- and optical luminosity- X-ray luminosity scaling relations, respectively.

bias induced by the limiting flux in the RASS observation, and probe whether the groups and clusters with strong X-ray emission have different galaxy populations from those of the same optical component but without strong X-ray emission.

5.1. *Unbiased scaling relations*

As shown in Section 4.1, $M_{*,c}$, $M_{\rm st}$, L_c and L_G are all strongly correlated with L_X, albeit with relatively large scatter. And we did not find strong correlations between L_X with other optical properties, e.g, the color and concentration of the central galaxies, the magnitude and luminosity gaps between the first and second most massive (luminous) galaxies, etc. Note also these relations are probed based on a small set of *observed* X-ray clusters. Because of the quite shallow flux limit of the RASS, the relations we obtained among them might suffer from the Malmquist bias. Here we try to find the unbiased scaling relations between $M_{*,c}$, $M_{\rm st}$ (or L_c , L_G) and L_X, assuming that the groups not observed in X-ray, apart from other selections like the bright star mask, are mainly due to the flux limit in the RASS observation.

In literature, there are claims about the existence of a genuine population of clusters that are X-ray underluminous (e.g., Castander et al. 1994; Balogh et al. 2011). However, as pointed out in a recent paper by Andreon & Moretti (2011) using Swift 1.4 Ms X-ray observations, there is no distinct populations of X-ray clusters, although the scatter in the X-ray luminosity is large. Therefore, the X-ray underluminous groups in our catalogue are expected to be systems whose X-ray luminosities are at the lower end of the scatter. As the optical group sample is more complete than the X-ray sample, we can use the observed number of X-ray clusters to constrain the *true* scaling relations and their scatter, in a manner that is not affected by Malmquist bias. To this end, we first measure the differential number distributions of X-ray clusters with respect to X-ray luminosity ($\hat{N}(L_{\rm X})$), redshift ($\hat{N}(z)$) and X-ray flux ($\hat{N}(F_X)$), respectively. These number distributions are obtained with the survey completeness of the X-ray clusters properly taken into account and with only X-ray clusters brighter

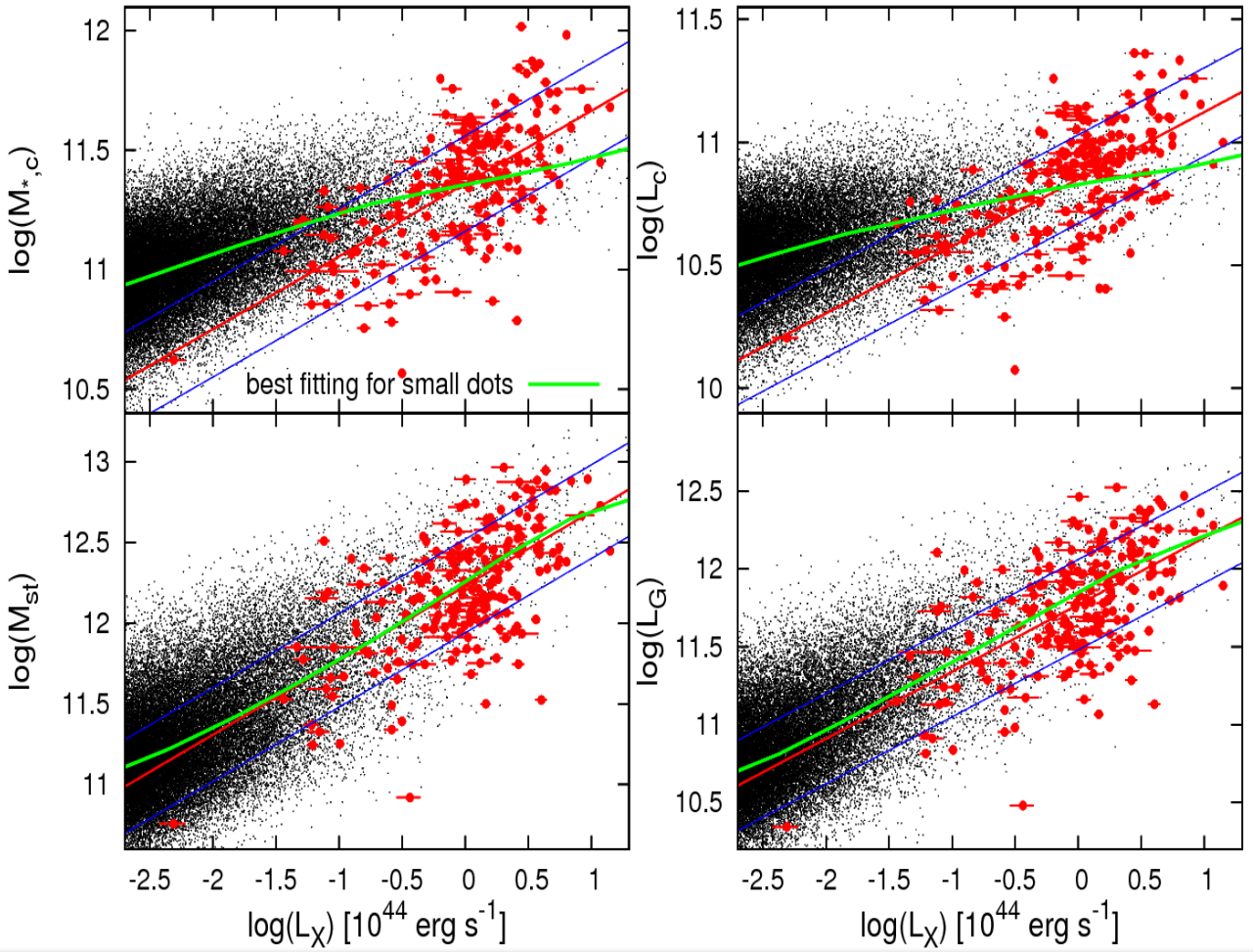

FIG. 9.— The distributions of stellar masses (upper-left panel) and luminosities (upper-right panel) of central galaxies, characteristic stellar masses (lower-left panel) and luminosities (lower-right panel) of groups as a function of X-ray cluster luminosity $\log L_{\rm X}$. Here big dots and solid straight lines are the results for the observed X-ray clusters (same as those shown in the upper panels of Figs 2 and 3). The small dots show the distributions of all galaxy groups whose X-ray luminosities are assigned using the scaling relations (Eqs. 6 and 7). The curves are the resulting average $\log L_{\rm X}$ as a function of stellar mass or luminosity in consideration.

than 3.0×10^{-12} erg cm^{-2} s^{-1} and redshift $z\leq0.1$ being used. Here every X-ray cluster is counted with a weight $1/c/f_{sky}$ where c is the completeness factor and f_{sky} is the relative sky coverage with respect to the SDSS DR7 in consideration. The results are shown in Fig. 7 as open squares with (Poisson) errorbars. These measurements are then used to constrain the unbiased scaling relations.

Since the characteristic stellar mass (luminosity) and the stellar mass (luminosity) of central galaxy are not independent variables (the latter is included in the former), we use the characteristic stellar mass (luminosity) of satellite galaxies, defined as $M_{\rm sat}=M_{\rm st}-M_{*,c}$ ($L_{\rm sat}=L_{\rm G}-L_c$), to replace $M_{\rm st}$ as the third quantity in our scaling relation analysis. Assume that the X-ray luminosity depend on the stellar masses of the centrals and satellites as

$$\log L_X=\alpha+\gamma[\log(M_{*,c}+\beta M_{\rm sat})-12.0]\,, \qquad (6)$$

with lognormal scatter σ, and on the luminosities of the central and

$$\log L_X=\alpha'+\gamma'[\log(L_{\rm c}+\beta' L_{\rm sat})-12.0]\,, \qquad (7)$$

with lognormal scatter σ'. We apply these models to all of our galaxy groups. The resulting X-ray luminosities are then properly converted into X-ray fluxes in the observed band taking into account the luminosity distances and negative average K corrections assuming an average X-ray temperature 5.0keV (Böhringer et al. 2004). From this 'X-ray group catalogue', we calculate the same quantities as shown in Fig. 7 with respect to X-ray luminosity ($N(L_{\rm X})$), redshift ($N(z)$) and X-ray flux ($N(F_X)$), respectively. Here taking into account the scatter in $\log L_X$ of the observed X-ray clusters, we set $\sigma=\sigma'=0.67$. Thus obtained data, together with those direct measurements from the observed X-ray clusters, are used to constrain the scaling relations. The goodness-of-fit of each model is described by its χ^2 value defined by

$$\chi^2=\sum\left[\frac{N(L_{\rm X})-\hat{N}(L_{\rm X})}{\Delta\hat{N}(L_{\rm X})}\right]^2+\sum\left[\frac{N(z)-\hat{N}(z)}{\Delta\hat{N}(z)}\right]^2 +\sum\left[\frac{N(F_X)-\hat{N}(F_X)}{\Delta\hat{N}(F_X)}\right]^2. \qquad (8)$$

Here $\hat{N}$ and $\Delta\hat{N}$ are the observed average number distribution and error of X-ray clusters, respectively.

To obtain the best fit and the freedom of the model parameters, we follow Yan, Madgwick & White (2003; see also van den Bosch et al. 2005) and use a Monte-Carlo Markov Chain (hereafter MCMC) to fully describe the likelihood function in our multi-dimensional parameter space. We start our MCMC from an initial guess and allow a 'burn-in' of 1000 random walk steps for the chain to equilibrate in the likelihood space. At any point in the chain we generate a new trial model by drawing the shifts in its three free parameters from three independent Gaussian distributions. The probability of accepting the trial model is

$$P_{\rm accept} = \begin{cases} 1.0 & \text{if } \chi^2_{\rm new} < \chi^2_{\rm old} \\ \exp[-(\chi^2_{\rm new} - \chi^2_{\rm old})/2] & \text{if } \chi^2_{\rm new} \geq \chi^2_{\rm old} \end{cases} \quad (9)$$

with the χ^2 measures given by eq. (8).

We construct a MCMC of 1 million steps, with an average acceptance rate of ~ 25 percent. In order to suppress the correlation power between neighboring models in the chain, we thin the chain by a factor 100. This results in a final MCMC consisting of 10000 independent models that properly sample the full posterior distribution. The contours in Fig. 8 plot the resulting projected 2-D distributions of the parameters, with the best-fit values indicated by a cross. The outer two level of contours correspond to the projected confidence regions of the 95% and 68% sets of parameters with smaller χ^2. And the best fit values, which have the smallest χ^2 value, are $[\alpha, \beta, \gamma] = [-0.26^{+0.15}_{-0.13}, 0.26^{+0.04}_{-0.02}, 2.90^{+0.16}_{-0.2}]$, and $[\alpha', \beta', \gamma'] = [-0.15^{+0.10}_{-0.10}, 0.72^{+0.06}_{-0.09}, 2.38^{+0.13}_{-0.14}]$, respectively. Here the superscript and subscript indicate the 68% confidence level of each best fit parameter while others are fixed. Note however, as the satellite components are in general correlated with the central galaxy, both of which increase with the increasing of the host halo mass, currently we are not able to put tight constraints on the β (or β') parameter indeed, as indicated by the very extended 2-D confidence contours. We note, in case one get a more reliable constraint on β (or β') that significantly deviates from our best fit value, one can get the updated $[\alpha, \gamma]$ (or $[\alpha', \gamma']$) from the 2-D confidence contour plots of the parameters.

Note that in constraining the scaling relations individual L_X of X-ray clusters are not used, as they might be biased tracers of the total X-ray cluster/group population in question. Rather we use the observed number of clusters as our constraints. The best fit differential numbers of X-ray clusters are shown as the solid and dotted lines in Fig. 7 for the cases where scaling relations are based on group stellar masses and luminosities, respectively. The shaded areas represent the 68% ranges of the 10000 MCMC independent model predictions.

Thus obtained scaling relations can be used to 'predict' the X-ray luminosities of clusters. As an example, we have applied Eqs. (6) and (7) to all of our galaxy groups, and use the resulting X-ray luminosities for all groups to check possible Malmquist bias in the observed X-ray sample in Figs. 2 and 3. In Fig. 9, we compare the distributions of the observed X-ray clusters and the one we 'predicted' from the optical galaxy groups. The small dots in each panel show the predicted distribution of all groups. Here the scaling relations and the corresponding lognormal scatters are applied to the stellar masses (left panels) and luminosities (right panels), respectively. For comparison, in each panel, we also show using solid curves the resulting average stellar mass or luminosity in consideration as a function of $\log L_{\rm X}$. It is clear that the observed X-ray clusters do suffer significantly from the Malmquist bias in the $M_{*,c} - L_X$ (or $L_c - L_X$) relation, especially at the low-mass end where the overall relation is flatter than the X-ray selected groups. Contrary to the case of the $M_{*,c} - L_{\rm X}$ relation, the predicted $M_{\rm st} - L_{\rm X}$ relation for X-ray clusters is in good agreement with the overall distribution of all groups, suggesting that in this case our best-fit linear regression is not strongly affected by Malmquist bias.

Finally, we note that the scaling relations obtained above are based on the assumption that there are no distinct populations of X-ray luminous and underluminous groups (see e.g. Andreon & Moretti 2011). If a significant fraction of the optical groups/clusters belonged to an X-ray underluminous population, then the scaling relations for the X-ray luminous groups/clusters would be different.

5.2. *The difference between the groups with and without strong X-ray emission*

In this subsection, we proceed to probe if those groups and clusters with strong X-ray emission have different galaxy populations from those without strong X-ray emission. For this purpose, we first check the distribution of X-ray clusters with respect to the survey flux limits. The left panel of Fig 10 plots the X-ray luminosities of the 201 X-ray clusters in our sample versus their redshifts. The dot-dashed and dashed lines mark roughly the two flux limits of the original X-ray samples, $F_X = 1.0 \times 10^{-12}\,{\rm erg\ cm^{-2}\ s^{-1}}$ and $F_X = 3.0 \times 10^{-12}\,{\rm erg\ cm^{-2}\ s^{-1}}$, respectively. Here an average K-correction, assuming $T_{\rm X} = 5$ keV, is used to convert X-ray flux to X-ray luminosity (Böhringer et al. 2004). In order to see whether or not the groups without detected X-ray emission are indeed distinct from the X-ray clusters, we plot in the middle panel of Fig. 10 the X-ray luminosities, inferred from the scaling relations with σ set to zero[13], for all groups in the SDSS DR7 group catalog versus the group redshifts. The groups that are linked to X-ray clusters are indicated using the same symbols as in the left panel, while other groups are shown as small dots. As an illustration, the two curves indicating the X-ray flux limits of the X-ray data are plotted as well. Because of the relatively large scatter in the scaling relation, the groups with X-ray detections do not obey these 'flux limits'. If there is zero scatter in the scaling relation, all groups above these flux-limits would be in our X-ray cluster sample, while those below it would have evaded detection. As one can see, some of our X-ray clusters have predicted L_X that are below the flux limits, and so their true X-ray luminosities are significantly scattered upwards relative to the prediction. On the other hand, a large number of groups with predicted L_X above the flux limits are not detected in X-rays (by ROSAT). This does not come as a surprise, as it is well known that the ob-

[13] As Eqs. 6 and 7 yield almost the same L_X, we use the former to make our prediction.

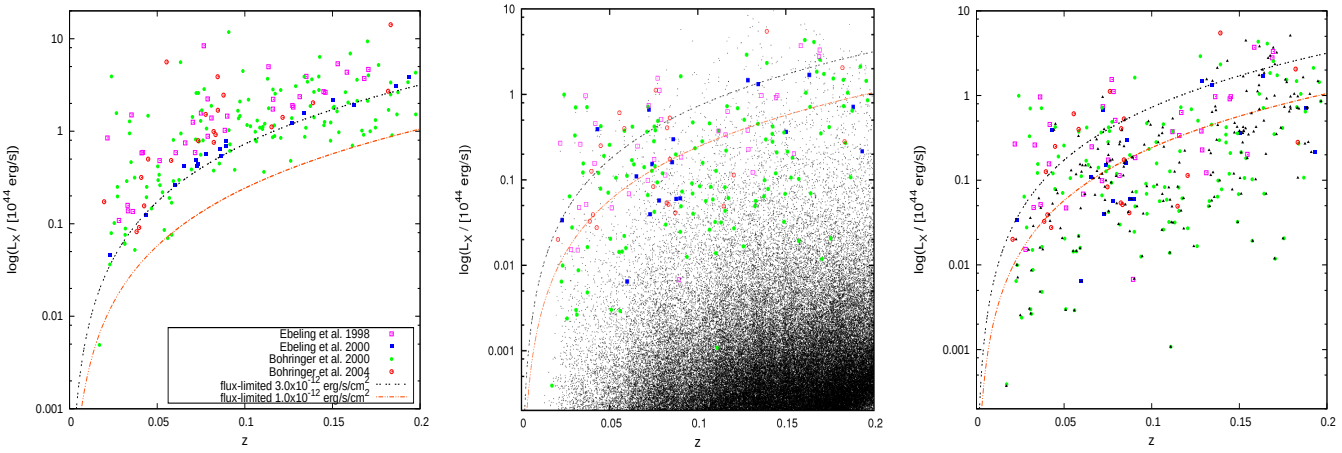

FIG. 10.— Left panel: the redshift v.s. X-ray luminosity distribution of all the X-ray clusters from different sources (symbols). The two lines correspond to the two flux limits, as indicated. Middle panel: the redshift v.s. X-ray luminosity distribution of groups with their X-ray luminosities predicted with the scaling relation (Eq.6) assuming zero scatter. For groups that are linked to X-ray clusters, which are shown as symbols, the distribution is quite different from that shown in the left panel. Right panel: the same as the middle panel, but here for a controlled sample of galaxy groups, constructed by matching a galaxy group without X-ray detection to the one with X-ray detection, according to its redshift and predicted X-ray luminosity L_X.

served L_X contains a significant amount of scatter with respect to their optical counterparts, as modelled in our full scaling relations. The main point of this exercise is to demonstrate that a large number of (massive) groups apparently have X-ray luminosities that are significantly below those of the 201 X-ray clusters in our sample, a point that has been made numerous times before (e.g., Castander et al. 1994; Lubin, Mulchaey & Postman 2004; Stanek et al. 2006; Popesso et al. 2007; Castellano et al. 2011; Balogh et al. 2011).

To investigate the difference between the groups with and without strong X-ray emissions properly, we construct a controlled group sample to prevent (or reduce) the influence of Malmquist bias. For an X-ray cluster at redshift z, we first obtain its model X-ray luminosity L_X using the scaling relation with zero scatter. We then search, among all groups without X-ray detections, the one that has the same (or similar) predicted X-ray luminosity and redshift as the X-ray cluster in question. We do this for all the X-ray clusters and produce a control sample of 201 groups without X-ray detections. Note that because of the RASS selection effects, not all the X-ray clusters are detected. And the groups not linked with known X-ray clusters are not necessary X-ray under-luminous. To avoid the false search of the controlled X-ray under-luminous groups, we require that each group in the controlled sample should also fulfill the following criteria: i) one can not find any X-ray sources, on the RASS map (and PSPC or HRI, if they are available), with signal-to-noise ratio $S/N > 3.0$ around the center of this group within a radius of 30 arcmins or the size of its r_{500c} whichever is larger. And ii) in the same region one can not find any cluster records in all published ROSAT-based catalogue. Otherwise, we reject this group until we find the control group that fulfill those two criteria for each X-ray cluster. Since the matched pairs have similar predicted L_X, their $M_{*c} + \beta M_{\rm sat}$ should also be similar. The right-hand panel of Fig. 10 shows the distribution of these groups (triangles) in the L_X - z plane, compared to that of the X-ray clusters (other symbols).

Using this control sample, we now examine whether groups that are under-luminous in X-ray emission have a different galaxy population (in a statistical sense) from that of X-ray luminous groups of similar masses at similar redshifts. Fig. 11 shows various optical group properties as function of group mass for both the sample of X-ray clusters (filled squares) and our control sample (open circles). These include the stellar mass of the central galaxies (upper left-hand panel), the r-band luminosity of the central galaxies (upper right-hand panel), the $^{0.1}(g-r)$ color of the central galaxies (middle left-hand panel), the concentration of the central galaxies (middle right-hand panels), and the stellar mass and luminosity gaps (lower left-hand and right-hand panels, respectively). None of these reveals any indication for a significant difference between X-ray luminous and X-ray under-luminous groups.

Next, we compare the conditional luminosity functions (CLF; see Yang, Mo & van den Bosch 2003), of the two samples. For this purpose we first divide the groups in the control sample into four mass bins (A3-D3), using the same M_G bins as in A1-D1 for the X-ray cluster sample. For each of the subsamples A1-D1 and A3-D3 we determine the CLF using the same method as outlined in Yang et al. (2008). The results are shown in Fig. 12 as symbols with error bars for A1-D1 (filled for centrals, open for satellites) and as histograms for A3-D3, where the error bars have been obtained from 200 bootstrap re-samplings of all the groups in consideration. Different panels correspond to different subsamples (different bins in halo mass, M_G), as indicated. Note that since the halo masses of the groups are estimated using $M_{\rm st}$ for all member galaxies with $^{0.1}{\rm M}_r - 5\log h \leq -19.5$, as expected, the CLFs between the two samples at bright end with $^{0.1}{\rm M}_r - 5\log h \leq -19.5$ are quite similar in both the central and satellite components. However, at the fainter end, a significant difference between the two samples is apparent: the groups that are X-ray luminous on average have more satellites than groups of the same mass that are under-luminous.

The left-hand panel of Fig. 13 shows the red fractions of satellite galaxies as function of group mass, M_G, for both group with (open squares) and without (open cir-

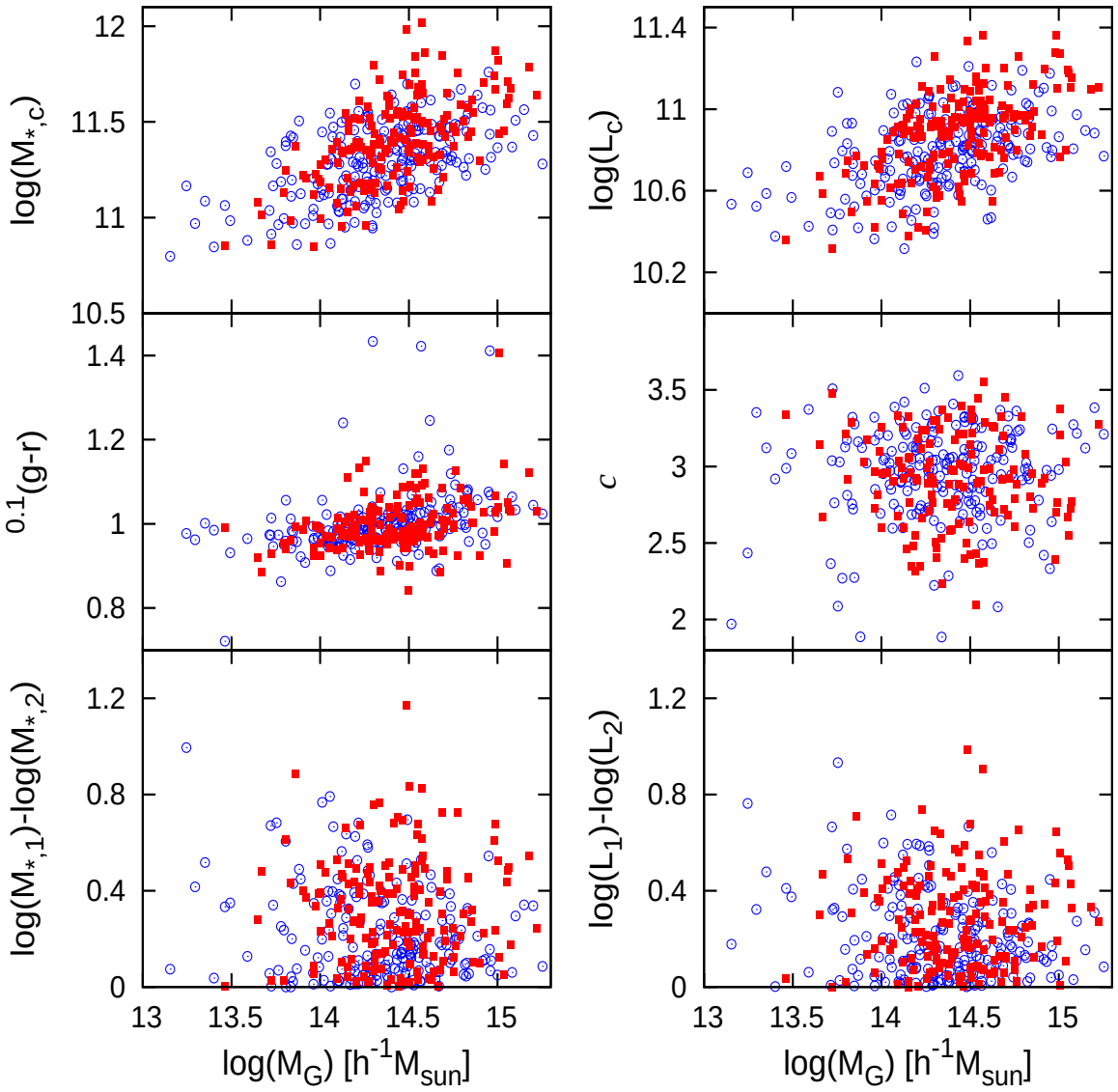

FIG. 11.— The optical properties of groups with (filled squares) and without (open circles) strong X-ray emissions. The latter are shown only for galaxy groups in the controlled sample.

cles) strong X-ray emission. Here we have used the same criteria as in Yang et al. (2008) to separate the galaxies into red and blue populations. There is a weak indication that groups without strong X-ray emission have lower red fractions, especially at lower masses, in quantitative agreement with the findings by Popesso et al. (2007) based on a significantly smaller sample of X-ray clusters. The right-hand panel of Fig. 13 compares the line-of-sight velocity dispersion (see Y07 for the detail of this measurement) of the satellite galaxies for the two samples, as function of the group mass M_G. Here we have only used groups with at least 8 members. For haloes with $M_G \gtrsim 10^{13.5}\ h^{-1}\mathrm{M}_\odot$ there is no indication that $\sigma_{\rm sat}$ is different for systems with or without strong X-ray emission. At the low mass end, however, there is a hint that groups in the X-ray under-luminous control sample have smaller values of $\sigma_{\rm sat}$ than their X-ray luminous counterparts. However, since this is based on only a handful of clusters, larger samples are required before any definite conclusion can be reached.

Finally, we check the large scale environments of the groups in our control sample. The asterisks in Fig. 6 indicate the average galaxy surface number density within $2.5\ h^{-1}\mathrm{Mpc} < r_{\rm p} < 5\ h^{-1}\mathrm{Mpc}$ (measured using the method described in Section 4.3) as a function of group mass M_G. A comparison with the X-ray clusters (solid squares) shows that there is no indication that groups or clusters that are under-luminous in X-rays reside in a different environment than their X-ray luminous counterparts of the same mass.

6. CONCLUSIONS

Galaxy clusters are the largest known gravitationally bound objects. Apart from their power on the cosmological studies, one can take advantage of the cross-identification between X-ray clusters and optical groups to understand the formation and evolution of galaxies in these densest regions in the large-scale structure. In this paper, we have extracted and refined an X-ray cluster sample from the ROSAT broadband (0.1-2.4 keV)

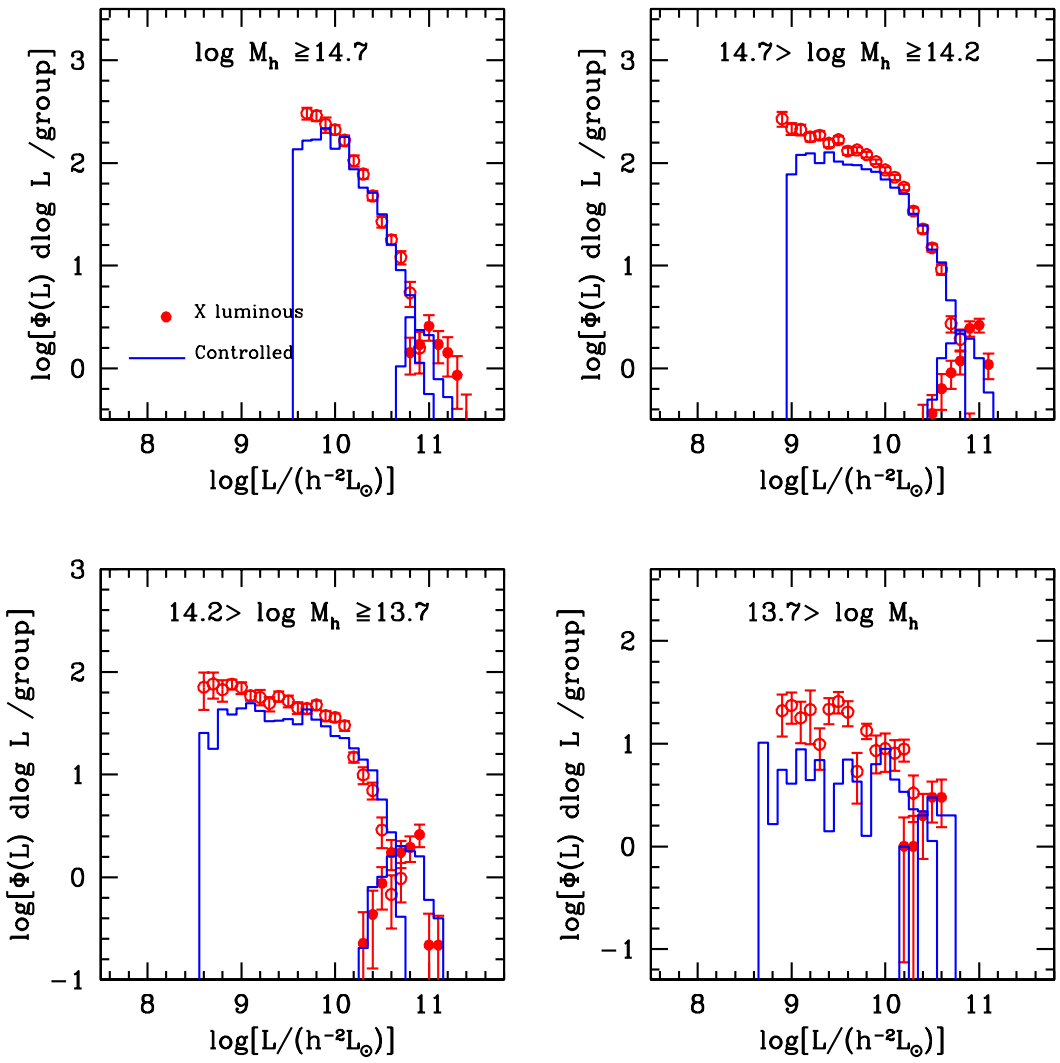

FIG. 12.— The conditional stellar mass functions of groups with (circles) and without (histograms) strong X-ray emissions. The contribution of central and satellite galaxies are plotted separately. The error bars are obtained from 200 bootstrap resampling of all the groups in consideration.

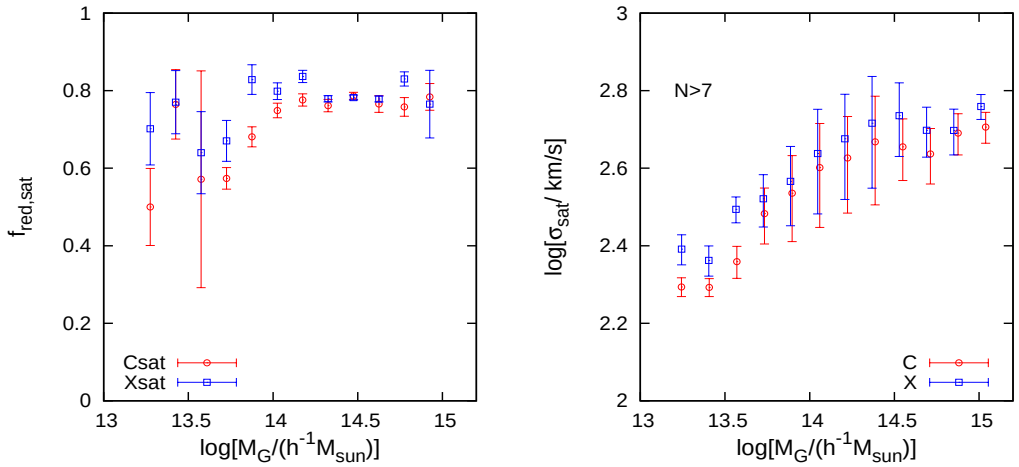

FIG. 13.— Left panel: the red fraction of satellite galaxies in groups with (squares) and without (circles) strong X-ray emission. Right panel: the velocity dispersion of satellite galaxies in groups with (squares) and without (circles) strong X-ray emission. The error bars are obtained from 200 bootstrap resampling of all the groups in consideration.

archive and matched them to the optical group catalogs constructed from the SDSS DR7. Since the galaxy groups are selected from the spectroscopic data, so that group memberships are reliable even for relatively low-mass systems, this cross-matched catalog is useful to probe galaxy formation and evolution in clusters. With this cross-identified sample, we have analyzed the optical and X-ray properties of galaxy clusters, and the correlation between them. Our main results are summarized as follows.

1. We have made an eyeball check of the central galaxies that are linked with X-ray clusters in the SDSS DR7 sky coverage. The optical groups are then linked with the X-ray clusters according to their central galaxies.

2. We have checked the general correlation between the optical and X-ray properties for all the X-ray clusters, and found that the stellar mass (or r-band luminosity) of the central galaxy is correlated with the X-ray luminosity.

3. The characteristic group stellar masses (or luminosity) used in Y07 to estimate the halo masses are also in good correlation with the X-ray luminosity to $L_{\rm X}^{0.46}$ (or $L_{\rm X}^{0.43}$ for r-band luminosity) with 1-σ scatter ~ 0.67 in $\log L_{\rm X}$.

4. Taking into observed X-ray flux limits and the quite large scatter ($\sigma \sim 0.67$) in the $\log L_{\rm X}$, We have obtained unbiased scaling relations between the X-ray luminosity and the group stellar masses (or luminosities) as: $\log L_X = -0.26 + 2.90[\log(M_{*,c} + 0.26M_{\rm sat}) - 12.0]$ ($\log L_X = -0.15 + 2.38[\log(L_c + 0.72L_{\rm sat}) - 12.0]$).

5. We have compared two sets of halo masses for the X-ray clusters, and found that the cluster mass $M_{\rm X}$ estimated from their X-ray luminosity are in general agreement with the group mass estimated from the stellar mass, $M_{\rm G}$. Quite interestingly, the systematical difference between the two sets of halo mass can be used to make simple cosmological probes.

6. Dividing the clusters into four subsamples of different $M_{\rm G}$ (or $M_{\rm X}$), we have investigated the surface number density of galaxies in and around the X-ray clusters. We found that X-ray clusters with larger $M_{\rm G}$ (or $M_{\rm X}$) live in more dense regions and are more strongly clustered. The strength is in general agreement with the CDM halo model prediction.

7. By comparing various properties of groups that are X-ray luminous or under-luminous, we found that groups linked with the X-ray clusters tend to have more faint member satellite galaxies. The X-ray luminous groups in general have larger red fraction of satellite galaxies.

8. The last but not the least, the cross-identified X-ray cluster catalog with 201+2 entries is provided in Appendix B to the public.

ACKNOWLEDGEMENTS

We thank the anonymous referee for helpful comments that greatly improved the presentation of this paper. This work is supported by grants from NSFC (Nos. 10821302, 10925314, 11128306, 11121062) and the CAS/SAFEA International Partnership Program for Creative Research Teams (KJCX2-YW-T23). HJM would like to acknowledge the support of NSF AST-0908334. WY is supported by the Fundamental Research Funds for the Central Universities,NSF-10903020, Research Foundation for Talented Scholars.

APPENDIX

A. CHECK THE DUPLICATIONS AND MERGING PAIRS

From the total 206 X-ray cluster entries in the SDSS DR7 sky coverage, we checked their coordinates and found that the following X-ray cluster pairs are un-resolvable in their X-ray images. In addition, we find each of these pairs points to the same central galaxy.

- **SDSS J100031.02+440843.3** and **RBS 0819**: Cross-identified through name RX J1000.4+4409 (or RXC J1000.5+4409).

- **NGC 4325** and **RX J1223.0 + 1037**: The X-ray source RX J1223.0+1037 is probably associated with NGC 4325 (see Crawford et al. 1999 and the NED website for detail).

- **NSCS J145254 + 164255** and **Abell 1983**: NED essential note shows that NSCS J145254 +164255 may be associated with Abell 1983.

The sources in each of the above pairs are closely associated, but are not treated as the same X-ray cluster in the literature. Through cross-identification with the SDSS groups, we argue that the clusters in each pair actually belong to the same cluster. To avoid double counting, we remove the less massive cluster in each pair from our sample.

Once X-ray clusters are linked to central galaxies, it is straightforward to obtain their group counterparts according to the central galaxies. In most cases one X-ray cluster is associated with one optical group. However, the following two close X-ray cluster pairs share the same optical groups. The broadband X-ray images do show that sources in each of these 2 pairs are definitely separated and resolvable. We think the two pairs are merging clusters, and only keep the bigger one in each pair for our investigations. However, for completeness, the two less massive clusters are also included in our Appendix B.

- **NSCS J145254 + 164255** and **IC 4516**: NED essential note shows that NSCS J145254+164255 may be associated with Abell 1983 which cross-identifies with IC 4516. Note that IC 4516 is a galaxy. The central galaxies of NSCS J145254+164255 and IC 4516 are both located in the same SDSS group (with group ID. 9). $M_{\rm XL}/M_{\rm XS} = 2.0$ (the footnote 'XL'/'XS' means the larger/smaller one).

- **NSC J160433 + 174311** and **Abell 2151E**: Abell 2151E is the subcluster of ABELL 2151. NED essential note shows that NSC J160433+174311 may be associated with Abell 2151. More importantly, the central galaxies of Abell 2151E and NSC J160433+174311 are located closely in the same group (ID. 6). $M_{\rm XL}/M_{\rm XS} = 3.8$.

B. THE CATALOG OF X-RAY CLUSTER IN THE SDSS DR7 REGION

The contents of Table 1 are as follows.

Column (1): Sequence number
Column (2): Cluster name (cross-identified by NED).
Column (3-4): Right ascension (J2000) and Declination (J2000) of X-ray position in equatorial frame. Obtained from the literature (based on ROSAT database).
Column (5): Cluster redshift. The subscript indicates the reference (a: Ebeling et al. 1998; b: Ebeling et al. 2000; c: Böhringer et al. 2000; d: Böhringer et al. 2004). Column (6): Updated redshift (see Section 3). The subscript indicates whether this corresponds to the spectroscopic redshift of the cluster's central galaxy (1), or whether it derives from the nearest neighbors (2).
Column (7): ICM gas temperature, $T_{\rm X}$ in units of keV. A superscript 'e' indicates that $T_{\rm X}$ has been estimated from the $T_{\rm X} - L_{\rm X}$ relation by the author of the reference from which the redshift in Column (5) was taken.
Column (8): Intrinsic X-ray luminosity in the 0.1-2.4 keV band (in the cluster rest frame) in units of 10^{44}erg s^{-1}, taken from the same reference as the redshift in Column (5).
Column (9): the 1σ fractional uncertainty for the count rate, the X-ray flux and the X-ray luminosity.
Column (10): Cluster halo mass $\log[M_{\rm X}/(h^{-1}M_{\odot})]$, which is estimated using Eq. 3.
Column (11): Group ID (the ID of the optical group in the SDSS DR7 group catalog that is associated with the X-ray cluster).
Column (12): 10-based logarithm of the characteristic group luminosity, L_G [in $h^{-2}L_{\odot}$].
Column (13): 10-based logarithm of the group stellar mass, $M_{\rm st}$ [in $h^{-2}M_{\odot}$)].
Column (14): 10-based logarithm of the group halo mass, M_G [in $h^{-1}M_{\odot}$)].
Column (15): ID of the cluster's central galaxy in the NYU-VAGC. For clusters in which the central galaxy is also the most massive galaxy, the ID has a subscript (1). A subscript (0) indicates that the central galaxy is NOT the most massive galaxy in the cluster.
Column (16): Absolute magnitude of cluster's central galaxy in r-band (K+E corrected to $z = 0.1$, model magnitude).
Column (17): $^{0.1}(g-r)$ color of cluster's central galaxy.
Column (18): 10-based logarithm of the cluster's central galaxy, $M_{*,c}$ [in $h^{-2}{\rm M}_{\odot}$].
Column (19): Offset in arcmins between the central galaxy and the X-ray cluster position listed in Columns (3) and (4).

Quantities without reliable measurements are denoted by '−'.

REFERENCES

Abazajian, K. et al. , 2009, ApJS, 182, 534
Abell, G. O., 1958, ApJS, 3,211
Abell, G. O., Corwin. H. G. Jr., & Olowin, R. P. 1989, ApJS, 70,1
Allen S.W., Edge A.C., Fabian A.C., Böhringer H., Crawford C.S., Ebeling H., Johnstone R.M., Naylor T.N., Schwarz R.A., 1992, MNRAS, 259, 67
Andreon, S., & Moretti, A. 2011, arXiv:1109.4031
Arnaud, M., Pratt, G. W., Piffaretti, R., et al. 2010, A&A, 517A,92A
Bahcall, N. A. 1977, ApJ, 217, L93
Balogh, M. L., Mazzotta, P., Bower, R. G., et al. 2011, MNRAS, 412, 947
Blanton, M. R., et al. 2005, AJ, 129, 2562
Böhringer et al., 2000, ApJS, 129, 435
Böhringer et al., 2004, A&A, 425, 367
Böhringer et al., 2007, A&A, 469, 363
Castander, F. J., Ellis, R. S., Frenk, C. S., Dressler, A., & Gunn, J. E. 1994, ApJ, 424, 79
Castellano, M., Pentericci, L., Menci, N., et al. 2011, A&A, 530, A27
Chen, J. 2008, A&A, 484, 347
Choi, Y.Y., Han, D.H., Kim, S. S. 2010, JKAS, 43, 191-200
Collister, A. A., & Lahav, O. 2005, MNRAS, 361, 415
Corwin, H. G. 1974, AJ, 79, 1356
Crawford C.S., Edge A.C., Fabian A.C., Allen S.W., Böhringer H., Ebeling H., McMahon RG., Voges W., 1995, MNRAS, 274, 75
Crawford, C.S., Allen, S.W., Ebeling, H., Edge, A.C. & Fabian, A.C., 1999, MNRAS, 306, 857 (C99)
Dai, X., Kochanek, C. S., & Morgan, N.D. 2007, ApJ, 658, 917
Donahue, M., et al. 2001, ApJ, 552, L93
Donahue, M., et al. 2002, ApJ, 569, 689
D'Onghia, E., Sommer-Larsen, J., Romeo, A. D., Burkert, A., Pedersen, K., Portinari, L., & Rasmussen, J. 2005, ApJ, 630, L109
Ebeling, H., Voges, W., Böhringer, H., Edge, A. C., Huchra, J. P., & Briel, U. G. 1996, MNRAS, 281, 799
Ebeling, H., Edge, A. C., Böhringer H., Allen, S. W., Crawford, C. S., Fabian, A. C., Voges, W., & Huchra, J. P. 1998, MNRAS, 301, 881
Ebeling, H., Edge, A. C., Allen, S. W., Crawford, C. S., Fabian, A. C., & Huchra, J. P. 2000, MNRAS, 318, 333
Edge, A. C., & Stewart G. C. 1991, MNRAS, 252, 428
Evans, I.N. et al., 2010, ApJS, 189,37
Forman, W., Kellogg, E., Gursky, H., Tananbaum, H., & Giacconi, R., 1971, ApJ, 138, 309
Gilbank, D. G., Bower, R. G., Castander, F. J., & Ziegler, B. L. 2004, MNRAS, 348, 551
Hansen, Sarah M., Sheldon, Erin S., Wechsler, Risa H., Koester, Benjamin P., 2009, ApJ, 699, 1333
Hao, J., et al. 2010, ApJS, 191, 254
Hudson, D. S., Mittal, R., Reiprich, T. H., Nulsen, P. E. J., Andernach, H., & Sarazin, C. L. 2010, A&A, 513, A37
Jones, C., & Forman, W., 1999, ApJ, 511, 65
Kellogg E., Gurcky, H., Leong, C., Scherier, E., Tananbaum, H., & Giacconi, R., 1971, ApJ, 165, L49
Kochanek, C. S., White, M., Huchra, J., Macri, L., Jarrett, T. H., Schneider, S. E., & Mader, J. 2003, ApJ, 585, 161
Koester, B. P., et al. 2007a, ApJ, 660, 221
Koester, B. P., et al. 2007b, ApJ, 660, 239
Komatsu, E., et al. 2011, ApJS, 192, 18
Leauthaud, A., et al. 2010, ApJ, 709, 97
Lin, Y.-T., Mohr, J. J., & Stanford, S. A. 2004, ApJ, 610, 745
Lubin, L. M., Mulchaey, J. S., & Postman, M. 2004, ApJ, 601, 9
Maccio, A. V., Dutton, A. A., van den Bosch, F. C., Moore, B., Potter, D., & Stadel, J. 2007, MNRAS, 378, 55

TABLE 1
THE CATALOGUE OF 204 X-RAY CLUSTERS AND THEIR ASSOCIATED GROUPS AND GALAXIES

No.	X-ray cluster ID	R.A.	Dec	z_X	z_X^c	T_X	L_X	L_X^{Err}	M_X	Gr ID	L_G	$M_{\rm st}$	M_G	Gal ID	M_r	$color$	M_*	Ofs
(1)	(2)	(3)	(4)	(5)	(6)	(7)	(8)	(9)	(10)	(11)	(12)	(13)	(14)	(15)	(16)	(17)	(18)	(19)
1	ABELL 0085	10.4587	-9.3019	0.0555_d	0.0554_1	6.90^e	5.581	0.032	14.935	11	12.062	12.468	14.575	359832_1	-22.797	0.981	11.505	0.12
2	1RXS J011006.0+135849	17.5229	13.9804	0.0581_c	0.0583_1	——	0.076	0.295	13.874	93	11.729	12.156	14.291	148784_1	-21.787	0.992	11.146	0.60
3	WBL 032	18.2741	15.5170	0.0442_c	0.0469_1	2.30^e	0.223	0.141	14.142	100	11.729	12.250	14.379	153588_0	-21.971	0.940	11.113	2.48
4	ABELL 0168	18.8000	0.3300	0.0450_d	0.0448_1	2.60	0.497	0.093	14.341	25	11.893	12.287	14.410	1765793_1	-22.131	0.974	11.223	7.04
5	SDSS CE J020.508463+00.332940	20.4929	0.3575	0.1756_c	0.1745_1	——	1.095	0.311	14.502	20144	11.967	12.441	14.548	2096076_1	-22.967	1.055	11.638	1.76
6	RXC J0137.2-0911	24.3140	-9.2028	0.0409_d	0.0409_2	——	0.315	0.084	14.229	129	11.498	11.899	14.050	3000001_1	-21.773	0.943	11.154	0.31
7	ABELL 0295	30.5829	-1.1204	0.0427_d	0.0425_1	——	0.155	0.137	14.055	244	11.400	11.842	13.991	1736056_1	-22.009	0.991	11.200	0.79
8	MaxBCG J111.48808+41.38519	111.5022	41.3821	0.1120_c	0.1113_1	4.30^e	1.204	0.158	14.542	1088	11.687	12.127	14.268	1731094_1	-22.959	1.006	11.579	0.87
9	RXC J0736.4+3925	114.1059	39.4332	0.1177_c	0.1180_1	——	2.575	0.088	14.728	2246	11.569	11.979	14.134	230665_0	-21.991	0.235	10.786	0.65
10	UGCl 104	116.6554	31.0136	0.0579_c	0.0582_2	——	0.169	0.210	14.071	515	11.394	11.813	13.962	833031_1	-21.290	0.943	10.848	1.71
11	1RXS J074809.3+183243	117.0394	18.5465	0.0400_c	0.0467_1	——	0.146	0.210	14.038	34	11.819	12.239	14.367	1140707_1	-22.460	0.968	11.342	0.71
12	WBL 154	117.8437	50.2125	0.0228_c	0.0238_2	1.80^e	0.079	0.296	13.893	213	11.129	11.594	13.722	1783916_1	-21.032	0.930	10.855	1.67
13	ABELL 0598	117.8500	17.5130	0.1894_b	0.1865_1	6.50^e	3.091	0.060	14.754	5667	12.111	12.657	14.762	1887146_1	-22.237	1.127	11.449	0.29
14	ABELL 0602	118.3510	29.3660	0.0621_a	0.0606_2	3.40^e	0.585	0.080	14.377	124	11.621	12.015	14.169	804064_1	-21.837	1.014	11.136	0.71
15	ZwCl 0755.8+5408	119.9284	54.0016	0.1032_c	0.1032_2	4.60^e	1.131	0.173	14.529	451	11.769	12.206	14.339	3000002_1	-22.599	0.887	11.385	0.64
16	ABELL 0616	121.0915	46.7823	0.1868_c	0.1868_1	——	1.520	0.367	14.579	93613	11.664	12.159	14.293	228159_1	-22.757	1.065	11.561	0.33
17	ABELL 0620	121.4304	45.6903	0.1353_c	0.1342_1	——	0.871	0.209	14.456	2623	11.543	12.117	14.260	218899_1	-21.906	1.150	11.353	0.36
18	ABELL 0635	122.7599	16.7349	0.0925_c	0.0942_2	——	0.383	0.285	14.264	1883	11.173	11.746	13.889	2131539_1	-22.179	1.148	11.453	1.61
19	RX J0820.9+0751	125.2574	7.8660	0.1100_c	0.1101_2	4.40^e	1.055	0.155	14.510	1293	11.457	11.911	14.063	1128297_1	-21.704	0.890	11.131	0.21
20	ZwCl 0822.8+4722	126.3761	47.1299	0.1267_c	0.1290_1	7.10^e	3.070	0.109	14.768	263	12.379	12.833	15.004	191508_1	-23.420	1.039	11.822	0.37
21	ABELL 0667	127.0190	44.7640	0.1450_a	0.1450_1	6.10^e	2.681	0.070	14.731	749	12.153	12.688	14.790	436039_1	-22.667	1.084	11.590	0.37
22	RXC J0828.6+3025	127.1621	30.4280	0.0503_c	0.0503_1	3.10^e	0.417	0.096	14.297	33	11.883	12.290	14.412	1067272_1	-22.523	0.964	11.395	1.83
23	NSC J084254+292723	130.7470	29.4760	0.1940_b	0.1937_1	7.00^e	3.889	0.070	14.809	43154	11.830	12.320	14.435	1155061_1	-22.765	1.042	11.555	1.39
24	RXC J0844.9+4258	131.2361	42.9817	0.0541_c	0.0540_1	——	0.086	0.186	13.905	955	11.242	11.662	13.797	832301_1	-21.957	0.953	11.132	0.31
25	MaxBCG J136.60704+10.36365	136.6140	10.3450	0.1328_b	0.1335_1	4.90^e	1.585	0.070	14.604	551	12.235	12.651	14.751	1827579_1	-22.486	0.992	11.371	1.19
26	ABELL 0744	136.8570	16.6540	0.0733_b	0.0728_1	3.00^e	0.416	0.060	14.290	331	11.455	11.882	14.031	2250692_1	-22.365	0.971	11.303	1.30
27	RXC J0909.1+1059	137.2832	10.9925	0.1751_c	0.1763_1	8.10^e	5.198	0.104	14.885	6093	12.255	12.823	14.989	2497007_1	-22.996	1.066	11.671	1.60
28	ABELL 0763	138.1240	15.9430	0.0851_a	0.0899_2	4.60^e	1.456	0.090	14.595	2594	11.067	11.500	13.616	2305668_1	-21.765	0.949	11.046	3.69
29	ABELL 0757	138.3570	47.6870	0.0514_a	0.0513_1	3.10^e	0.481	0.100	14.331	170	11.554	11.969	14.122	855554_1	-21.453	0.973	10.952	4.67
30	ABELL 0779	139.9220	33.7630	0.0230_b	0.0229_1	1.40^e	0.046	0.070	13.762	35	11.438	11.853	14.004	1158309_1	-22.136	0.923	11.188	1.61
31	RXC J0920.0+0102	140.0020	1.0401	0.0175_c	0.0170_1	——	0.005	0.237	13.209	3891	10.345	10.759	12.554	184191_1	-20.753	0.922	10.621	0.44
32	3C 219	140.2857	45.6437	0.1745_c	0.1746_1	——	1.320	0.216	14.548	35702	11.326	11.752	13.895	800906_1	-22.025	0.937	11.181	0.33
33	ABELL 0795	141.0238	14.1684	0.1357_c	0.1357_1	6.60^e	3.428	0.096	14.794	275	12.354	12.762	14.902	2348261_1	-22.429	0.925	11.296	0.27
34	ABELL 0853	145.5605	15.3865	0.1664_c	0.1641_1	5.80^e	2.131	0.140	14.669	67569	11.546	12.065	14.214	2484487_1	-22.817	1.065	11.594	0.34
35	ABELL 0845	146.0074	64.4117	0.1200_c	0.1205_1	——	0.848	0.168	14.453	3521	11.344	11.822	13.972	1703417_1	-22.456	1.020	11.397	0.60
36	MaxBCG J149.55144+23.77931	149.5430	23.7820	0.1471_c	0.1451_1	——	1.160	0.262	14.524	8110	11.692	12.107	14.250	2239218_1	-22.739	0.999	11.491	0.53
37	SDSS J100031.02+440843.3	150.1272	44.1543	0.1540_c	0.1532_1	5.20^e	1.655	0.127	14.609	2743	11.720	12.172	14.308	894438_0	-21.251	0.973	10.868	0.55
38	NSCS J100242+324218	150.6609	32.6995	0.0499_c	0.0505_1	2.60^e	0.296	0.111	14.212	161	11.322	11.760	13.903	1884461_1	-22.052	0.985	11.222	0.68
39	ABELL 0923	151.6647	25.9101	0.1162_c	0.1168_1	4.40^e	1.158	0.140	14.531	851	11.809	12.261	14.387	2173549_1	-23.106	0.988	11.615	0.23
40	ABELL 0961	154.0850	33.6410	0.1241_a	0.1272_1	5.20^e	1.899	0.080	14.651	729	11.969	12.395	14.502	1890546_1	-22.537	0.962	11.359	0.64
41	ABELL 0964	154.1503	24.8082	0.0811_c	0.1701_2	3.00^e	2.129	0.183	14.667	4565	11.946	12.476	14.582	3000003_1	-22.630	1.131	11.651	0.45
42	RX J1020.0+4100	154.9992	40.9873	0.0922_c	0.0914_1	3.80^e	0.613	0.164	14.381	596	11.590	12.050	14.202	1246123_1	-22.532	0.971	11.395	1.93
43	RX J1022.1+3830	155.5196	38.5120	0.0491_c	0.0530_1	2.20^e	0.219	0.283	14.137	105	11.706	12.130	14.269	1157141_0	-21.251	0.927	11.021	1.45
44	ABELL 0980	155.6170	50.1210	0.1582_a	0.1582_2	7.40^e	4.345	0.090	14.846	821	12.441	12.945	15.179	3000004_1	-22.986	1.122	11.785	0.93
45	MaxBCG J155.91636+49.14401	155.9220	49.1329	0.1440_c	0.1422_1	7.50^e	3.906	0.082	14.824	1413	11.979	12.427	14.531	871988_1	-22.838	0.974	11.513	0.75
46	ZwCl 1023.3+1257	156.4829	12.6852	0.1434_c	0.1423_1	6.20^e	2.787	0.094	14.741	5674	11.863	12.466	14.573	3000005_1	-23.646	1.091	12.017	0.52
47	MaxBCG J157.93473+35.04138	157.9317	35.0495	0.1259_c	0.1205_2	6.30^e	2.789	0.111	14.747	231	12.103	12.536	14.639	1891363_1	-22.269	1.022	11.318	0.52
48	RXC J1032.2+4015	158.0590	40.2470	0.0733_b	0.0776_1	3.20^e	0.568	0.070	14.366	387	11.541	11.971	14.123	1184055_1	-22.433	0.972	11.347	1.46
49	ABELL 1045	158.7469	30.6944	0.1407_c	0.1374_1	5.40^e	1.873	0.109	14.644	8073	11.504	11.964	14.115	2215203_1	-22.953	1.007	11.575	0.23
50	ABELL 1068	160.1829	39.9481	0.1372_c	0.1383_1	7.50^e	3.637	0.083	14.808	7318	11.602	12.023	14.177	1182121_1	-23.103	0.946	11.587	0.34

TABLE 1
CONTINUED

(1)	(2)	(3)	(4)	(5)	(6)	(7)	(8)	(9)	(10)	(11)	(12)	(13)	(14)	(15)	(16)	(17)	(18)	(19)
51	RX J1053.7+5450	163.4490	54.8500	0.0704_{a}	0.0716_{1}	3.30^{e}	0.588	0.080	14.376	146	11.712	12.114	14.256	797988_{1}	-21.476	0.965	10.959	2.99
52	NSCS J105344+165124	163.4530	16.8420	0.0856_{b}	0.0856_{2}	3.50^{e}	0.637	0.070	14.392	692	11.693	12.165	14.301	3000006_{1}	-23.386	0.969	11.799	0.64
53	ABELL 1139	164.5434	1.5865	0.0398_{d}	0.0382_{1}	2.10^{e}	0.082	0.200	13.897	37	11.759	12.192	14.329	278531_{1}	-21.681	1.031	11.262	1.09
54	ABELL 1132	164.6160	56.7820	0.1363_{a}	0.1351_{1}	7.10^{e}	3.919	0.100	14.827	708	12.166	12.650	14.750	799723_{1}	-22.674	0.998	11.474	1.30
55	ABELL 1173	167.3282	41.5624	0.0763_{c}	0.0748_{2}	3.30^{e}	0.558	0.116	14.362	422	11.512	11.963	14.114	1276712_{1}	-21.837	0.985	11.151	0.86
56	NGC 3551	167.4294	21.7620	0.0319_{c}	0.0318_{1}	1.90^{e}	0.089	0.143	13.919	330	11.143	11.547	13.671	2306474_{1}	-21.701	0.886	11.016	0.40
57	ABELL 1185	167.6950	28.7060	0.0314_{a}	0.0331_{1}	3.90	0.158	0.120	14.061	7	11.911	12.339	14.453	2205041_{0}	-21.204	0.890	10.754	1.25
58	ABELL 1190	167.9104	40.8424	0.0794_{c}	0.0781_{1}	3.80^{e}	1.070	0.103	14.522	62	11.963	12.396	14.502	1274637_{1}	-22.669	0.899	11.343	1.83
59	ABELL 1201	168.2250	13.4500	0.1688_{a}	0.1681_{1}	6.90^{e}	3.714	0.080	14.805	1800	12.377	12.884	15.058	1823070_{1}	-23.180	1.050	11.713	0.86
60	ABELL 1204	168.3324	17.5937	0.1706_{c}	0.1705_{1}	7.30^{e}	4.016	0.108	14.823	461365	11.131	11.525	13.645	2407813_{1}	-22.316	0.934	11.251	0.19
61	SDSS-C4-DR3 3043	168.8865	54.4350	0.0691_{c}	0.0695_{1}	——	0.386	0.138	14.273	104	11.747	12.140	14.277	965525_{1}	-22.520	0.935	11.326	2.29
62	RXC J1121.7+0249	170.4280	2.8184	0.0468_{c}	0.0511_{1}	——	0.339	0.118	14.245	58	11.634	12.054	14.205	288542_{1}	-21.290	0.991	11.061	4.89
63	SDSS-C4 3084	170.5604	67.2129	0.0560_{c}	0.0560_{1}	——	0.070	0.203	13.854	1253	10.911	11.328	13.408	251609_{1}	-21.271	1.004	10.913	0.59
64	RBS 0976	170.8049	19.5996	0.1042_{c}	0.1103_{2}	4.70^{e}	1.113	0.132	14.523	12646	11.161	11.683	13.821	2355104_{1}	-22.398	1.024	11.379	0.66
65	RXC J1123.9+2129	170.9912	21.4903	0.1904_{c}	0.1975_{2}	7.50^{e}	4.296	0.149	14.832	3671	12.259	12.843	15.009	2301899_{1}	-22.158	1.405	11.435	0.69
66	ABELL 1264	171.7530	17.1260	0.1267_{b}	0.1267_{2}	4.40^{e}	1.213	0.060	14.540	343	12.252	12.742	14.863	3000007_{1}	-22.715	1.003	11.551	0.31
67	ABELL 1291	173.0817	55.9789	0.0527_{c}	0.0515_{1}	2.40^{e}	0.261	0.123	14.181	672	10.953	11.341	13.425	835751_{1}	-20.965	0.982	10.781	1.13
68	ABELL 1302	173.3070	66.3990	0.1160_{a}	0.1160_{2}	5.10^{e}	1.737	0.070	14.631	299	11.921	12.396	14.503	3000008_{1}	-22.954	1.044	11.695	1.20
69	ABELL 1314	173.7480	49.0900	0.0338_{a}	0.0333_{1}	5.00	0.138	0.090	14.028	43	11.540	11.943	14.093	955566_{1}	-21.820	0.939	11.076	2.66
70	ABELL 1361	175.8762	46.3845	0.1167_{c}	0.1160_{1}	5.50^{e}	2.825	0.349	14.752	2051	11.474	11.935	14.085	1168647_{1}	-22.398	0.948	11.336	2.90
71	ABELL 1367	176.1520	19.7590	0.0214_{a}	0.0216_{1}	3.50	0.846	0.320	14.478	3	11.917	12.327	14.441	2330539_{0}	-21.382	0.941	10.905	11.61
72	ABELL 1366	176.2020	67.4130	0.1159_{a}	0.1161_{1}	5.60^{e}	2.213	0.070	14.691	224	12.076	12.507	14.611	229148_{1}	-22.582	0.936	11.371	2.95
73	ABELL 1413	178.8270	23.4075	0.1427_{c}	0.1427_{2}	8.90	6.364	0.064	14.945	5980	11.816	12.380	14.486	3000009_{1}	-23.573	1.087	11.983	0.19
74	ZwCl 1154.2+2435	179.2409	24.2581	0.1392_{c}	0.1395_{2}	5.20^{e}	1.414	0.129	14.574	3035	11.628	12.084	14.229	2263177_{1}	-22.252	0.979	11.276	0.52
75	ABELL 1437	180.1057	3.3336	0.1339_{c}	0.1339_{2}	7.40^{e}	3.889	0.086	14.826	1256	11.971	12.481	14.589	3000010_{1}	-23.239	1.096	11.861	0.81
76	RX J1201.9+5802	180.4997	58.0475	0.1031_{c}	0.1060_{2}	3.70^{e}	0.807	0.193	14.445	714	11.564	11.994	14.152	1200250_{0}	-22.037	0.927	11.160	1.21
77	2MASX J12025923+2836444	180.7615	28.6039	0.1341_{c}	0.1348_{1}	——	1.089	0.157	14.511	2182	11.591	12.036	14.189	2244173_{1}	-21.544	0.988	11.081	1.01
78	NSC J120403+280727	181.0133	28.1233	0.1631_{c}	0.1668_{1}	——	1.016	0.193	14.485	1104	12.462	12.890	15.065	2243047_{1}	-23.005	1.034	11.626	0.33
79	MKW 04	181.1049	1.9005	0.0199_{d}	0.0197_{1}	1.70	0.172	0.060	14.085	64	11.339	11.814	13.963	265118_{1}	-21.821	0.924	11.119	0.55
80	RBS 1066	181.3021	39.3493	0.0381_{c}	0.0371_{1}	2.30^{e}	0.315	0.074	14.231	1202	10.980	11.392	13.490	1850962_{0}	-20.425	0.992	10.566	0.55
81	NGC 4104 GROUP	181.6470	28.1800	0.0283_{a}	0.0282_{1}	1.80^{e}	0.109	0.090	13.970	85	11.239	11.670	13.807	2243092_{1}	-22.105	0.941	11.245	0.98
82	ZwCl 1207.5+0542	182.5783	5.3850	0.0748_{c}	0.0762_{1}	3.50^{e}	0.797	0.104	14.450	265	11.642	12.070	14.218	460946_{1}	-22.623	0.957	11.393	0.50
83	ZwCl 1215.1+0400	184.4192	3.6624	0.0766_{c}	0.0768_{1}	5.58^{e}	2.851	0.054	14.764	44	12.033	12.472	14.579	275461_{1}	-22.192	0.971	11.303	0.41
84	NGC 4325	185.7772	10.6240	0.0258_{c}	0.0255_{1}	1.80^{e}	0.102	0.078	13.955	555	10.838	11.254	13.308	947351_{1}	-21.379	0.961	10.895	0.17
85	RXC J1225.2+3213	186.3001	32.2291	0.0594_{c}	0.0592_{1}	——	0.290	0.125	14.204	570	11.230	11.653	13.788	1947851_{1}	-22.245	0.983	11.270	0.39
86	ABELL 1541	186.8667	8.8290	0.0896_{c}	0.0855_{2}	——	0.448	0.197	14.305	220	11.830	12.251	14.380	936475_{1}	-22.420	0.976	11.355	0.73
87	MaxBCG J186.96340+63.38475	186.9603	63.3830	0.1454_{c}	0.1455_{1}	——	1.259	0.155	14.544	1557	11.863	12.319	14.434	558570_{1}	-21.787	1.069	11.263	0.22
88	RXC J1229.9+1147	187.4966	11.7891	0.0852_{c}	0.0915_{2}	——	0.722	0.340	14.421	1063	11.499	11.912	14.065	1219366_{1}	-22.462	0.968	11.357	4.11
89	ABELL 1553	187.7000	10.5560	0.1652_{a}	0.1705_{1}	7.40^{e}	4.655	0.080	14.860	2765	12.406	12.820	14.980	947413_{1}	-23.436	0.981	11.739	0.62
90	ABELL 1589	190.3250	18.5510	0.0718_{a}	0.0704_{1}	4.60^{e}	1.251	0.110	14.562	30	12.109	12.522	14.625	2418936_{1}	-22.626	1.001	11.453	1.42
91	ABELL 1612	191.9300	-2.7921	0.1797_{d}	0.1818_{1}	——	2.691	0.340	14.721	2617	12.327	12.873	15.037	174632_{1}	-22.232	1.143	11.452	3.09
92	MACS J1255.5+3521	193.8781	35.3602	0.1585_{c}	0.1614_{1}	——	0.702	0.222	14.395	2976	12.170	12.618	14.714	1900466_{1}	-23.035	1.037	11.650	0.81
93	ABELL 1650	194.6712	-1.7569	0.0845_{d}	0.0845_{2}	6.70^{e}	3.863	0.061	14.837	89	12.018	12.469	14.576	3000011_{1}	-23.054	0.994	11.694	0.29
94	RBS 1198	194.9294	27.9386	0.0231_{c}	0.0239_{1}	8.00^{e}	3.910	0.124	14.855	1	12.182	12.591	14.693	2243552_{1}	-22.147	0.935	11.210	2.22
95	ABELL 1663	195.7112	-2.5062	0.0847_{d}	0.0823_{1}	——	0.754	0.219	14.435	84	11.980	12.408	14.514	166440_{1}	-22.627	0.993	11.444	0.77
96	1RXS J130303.2+575623	195.7614	57.9419	0.1961_{c}	0.1953_{2}	——	1.482	0.184	14.570	7144	12.140	12.645	14.746	1201353_{0}	-22.042	1.020	11.225	2.15
97	ABELL 1668	195.9398	19.2715	0.0643_{c}	0.0635_{1}	3.90^{e}	0.946	0.081	14.495	96	11.764	12.204	14.338	2361168_{1}	-22.521	0.997	11.393	0.26
98	ABELL 1672	196.1147	33.5920	0.1882_{c}	0.1873_{1}	6.30^{e}	2.635	0.153	14.715	5719	12.081	12.584	14.685	1895982_{1}	-22.626	1.010	11.452	0.31
99	ABELL 1677	196.4778	30.9065	0.1832_{c}	0.1832_{2}	6.90^{e}	3.369	0.116	14.776	3581	12.182	12.717	14.835	3000012_{1}	-22.666	1.049	11.577	0.98
100	MS 1306.7-0121	197.3208	-1.6126	0.0880_{d}	0.0833_{1}	——	0.914	0.151	14.482	545	11.504	11.942	14.092	169619_{1}	-22.526	0.988	11.395	0.80
101	RX J1311.1+3913	197.7710	39.2220	0.0720_{b}	0.0723_{1}	3.10^{e}	0.491	0.060	14.331	46	12.079	12.505	14.609	1836950_{1}	-22.855	0.968	11.496	0.93

TABLE 1
CONTINUED

(1)	(2)	(3)	(4)	(5)	(6)	(7)	(8)	(9)	(10)	(11)	(12)	(13)	(14)	(15)	(16)	(17)	(18)	(19)
102	ABELL 1689	197.8750	-1.3354	0.1832_{d}	0.1832_{2}	9.23^{e}	14.089	0.080	15.130	15382	11.892	12.448	14.554	3000013_{1}	-22.735	1.119	11.680	0.36
103	MaxBCG J197.94248+22.02702	197.9300	22.0267	0.1716_{c}	0.1715_{1}	——	0.998	0.173	14.479	4617	12.280	12.736	14.857	2307337_{1}	-23.036	1.003	11.613	0.75
104	NSCS J132014+330824	200.0350	33.1430	0.0362_{a}	0.0361_{1}	2.00^{e}	0.136	0.080	14.023	71	11.574	11.994	14.151	1896056_{0}	-21.444	0.971	10.945	1.58
105	ABELL 1716	200.2374	33.9041	0.1820_{c}	0.1820_{2}	——	1.701	0.150	14.608	5724	12.113	12.604	14.703	3000014_{1}	-22.395	1.006	11.420	0.42
106	RXC J1323.5+1117	200.8760	11.2960	0.0911_{b}	0.0895_{1}	3.60^{e}	0.690	0.080	14.411	598	11.545	11.974	14.128	1223762_{1}	-22.539	0.942	11.339	0.52
107	NGC 5129	201.0497	13.9792	0.0230_{c}	0.0230_{1}	——	0.036	0.171	13.701	152	11.150	11.530	13.651	1829896_{1}	-21.918	0.920	11.078	0.50
108	ABELL 1744	201.4572	59.3225	0.1515_{c}	0.1509_{1}	5.30^{e}	1.841	0.099	14.636	3214	11.825	12.319	14.434	922325_{1}	-22.812	1.025	11.541	0.47
109	SDSS CE J201.573563+00.213468	201.5743	0.2257	0.0826_{d}	0.0822_{1}	4.00^{e}	0.988	0.117	14.501	659	11.505	11.986	14.142	244060_{1}	-22.626	1.005	11.546	0.26
110	ABELL 1750	202.7081	-1.8728	0.0852_{d}	0.0879_{1}	——	2.440	0.116	14.723	703	11.482	11.948	14.098	571059_{1}	-22.185	1.013	11.285	0.67
111	MaxBCG J203.14997+54.31696	203.1671	54.3205	0.1017_{c}	0.1066_{1}	——	0.776	0.140	14.435	2779	11.309	11.768	13.912	969459_{1}	-22.603	0.990	11.428	1.05
112	ABELL 1767	204.0255	59.2079	0.0701_{c}	0.0701_{2}	4.10	1.429	0.054	14.595	48	11.955	12.392	14.499	3000015_{1}	-22.654	0.986	11.533	0.56
113	RXC J1339.5+1830	204.8952	18.5122	0.1140_{c}	0.1109_{1}	——	0.364	0.215	14.247	450979	10.481	10.920	12.803	2361474_{1}	-21.379	0.943	10.897	0.79
114	ABELL 1775	205.4740	26.3720	0.0724_{c}	0.0755_{1}	4.90	1.687	0.167	14.635	69	11.902	12.351	14.463	1993364_{1}	-22.579	0.961	11.531	1.16
115	ABELL 1773	205.5228	2.2275	0.0765_{d}	0.0734_{2}	3.90^{e}	0.786	0.129	14.447	262	11.655	12.079	14.225	268720_{1}	-22.038	0.962	11.182	1.04
116	ABELL 1795	207.2207	26.5956	0.0622_{c}	0.0633_{1}	5.10	5.572	0.028	14.933	28	11.983	12.392	14.498	2010099_{1}	-22.710	0.842	11.358	0.20
117	ABELL 1804	207.2582	49.3047	0.1665_{c}	0.1678_{1}	——	0.914	0.202	14.459	1457	12.306	12.717	14.836	1369451_{1}	-22.411	1.060	11.424	0.54
118	NSCS J134935+280633	207.3402	28.1036	0.0748_{c}	0.0748_{2}	5.10^{e}	1.293	0.082	14.569	65	11.985	12.437	14.541	3000016_{1}	-22.682	0.969	11.523	0.53
119	RXC J1351.7+4622	207.9398	46.3668	0.0625_{c}	0.0625_{1}	——	0.297	0.150	14.210	83	11.796	12.212	14.344	1208324_{0}	-22.152	0.967	11.239	0.92
120	RXC J1353.0+0509	208.2750	5.1580	0.0790_{a}	0.0789_{1}	3.90^{e}	0.882	0.090	14.474	55	12.025	12.476	14.583	527307_{1}	-22.739	0.998	11.496	0.51
121	ABELL 1814	208.5095	14.9231	0.1251_{c}	0.1268_{1}	5.00^{e}	1.389	0.160	14.573	459	12.032	12.469	14.576	2380213_{1}	-22.453	0.985	11.381	0.73
122	ABELL 1831	209.8020	27.9780	0.0612_{a}	0.0750_{2}	4.20^{e}	1.573	0.120	14.618	143	11.780	12.237	14.365	3000017_{1}	-22.746	0.961	11.539	0.66
123	ABELL 1885	213.4313	43.6634	0.0890_{c}	0.0909_{1}	4.60^{e}	1.029	0.078	14.509	900	11.391	11.841	13.991	1204948_{1}	-21.781	1.002	11.118	1.12
124	ABELL 1882	213.8092	-0.5010	0.1403_{d}	0.1389_{1}	——	2.018	0.200	14.662	287	12.522	12.964	15.222	65728_{1}	-23.009	1.030	11.640	1.52
125	SDSS CE J213.951309+00.256928	213.9650	0.2589	0.1259_{c}	0.1262_{1}	——	0.479	0.224	14.311	3770	11.312	11.745	13.887	75646_{1}	-21.602	0.978	11.004	0.70
126	RXC J1416.5+3045	214.1354	30.7621	0.1860_{c}	0.1840_{1}	——	0.904	0.232	14.452	20971	11.900	12.402	14.508	1919023_{1}	-22.390	1.091	11.462	2.20
127	RBS 1380	215.3981	49.5519	0.0716_{c}	0.0719_{1}	3.60^{e}	0.816	0.080	14.457	339	11.579	12.040	14.192	1380642_{1}	-22.394	0.997	11.370	0.08
128	ABELL 1902	215.4226	37.2958	0.1813_{c}	0.1574_{1}	6.60^{e}	2.642	0.108	14.724	18659	11.286	11.745	13.887	1292787_{1}	-22.221	0.983	11.255	2.14
129	RX J1423.1+2615	215.7922	26.2556	0.0375_{c}	0.0372_{1}	1.80^{e}	0.052	0.164	13.786	103	11.306	11.775	13.920	1971369_{1}	-21.612	1.006	11.207	0.61
130	RBS 1385	215.9685	40.2619	0.0822_{c}	0.0822_{1}	3.20^{e}	0.375	0.131	14.262	595	11.401	11.852	14.002	1245278_{1}	-22.212	0.989	11.279	0.29
131	MaxBCG J216.34368+63.19819	216.3447	63.1872	0.1394_{c}	0.1394_{1}	5.80^{e}	2.664	0.112	14.731	2250	11.878	12.431	14.533	3000019_{1}	-23.134	1.120	11.844	0.66
132	ABELL 1914	216.5068	37.8271	0.1712_{c}	0.1700_{1}	10.53^{e}	9.364	0.052	15.032	2411	12.359	12.891	15.073	1296192_{1}	-23.126	1.031	11.674	1.40
133	ABELL 1925	217.1171	56.8829	0.1051_{c}	0.1060_{1}	3.90^{e}	0.987	0.171	14.495	239	11.984	12.428	14.531	990388_{1}	-23.078	0.960	11.573	2.88
134	ABELL 1927	217.7794	25.6388	0.0908_{c}	0.0964_{2}	4.40^{e}	1.378	0.105	14.580	456	11.676	12.133	14.273	1980477_{1}	-21.997	0.940	11.177	0.31
135	ABELL 1930	218.1200	31.6330	0.1313_{a}	0.1313_{2}	5.80^{e}	2.362	0.080	14.703	2453	11.675	12.198	14.333	3000020_{1}	-22.980	1.060	11.718	2.43
136	WBL 518	220.1592	3.4765	0.0263_{c}	0.0273_{1}	3.29^{e}	0.198	0.087	14.118	22	11.597	12.034	14.188	487370_{1}	-22.001	0.970	11.168	1.33
137	NSC J144215+221740	220.5768	22.3048	0.0901_{c}	0.0972_{2}	4.80^{e}	1.463	0.090	14.594	684	11.588	12.024	14.178	1989751_{1}	-22.400	0.988	11.356	0.26
138	ABELL 1978	222.7750	14.6110	0.1460_{a}	0.1460_{1}	6.00^{e}	2.631	0.080	14.726	861	12.162	12.579	14.678	2385566_{1}	-22.782	0.972	11.472	0.85
139	NSCS J145254+164255	223.2449	16.6998	0.0444_{c}	0.0440_{2}	2.50^{e}	0.250	0.155	14.172	9	11.995	12.399	14.506	2345992_{0}	-21.297	0.938	10.857	0.88
140	ABELL 1986	223.2798	21.8947	0.1186_{c}	0.1170_{2}	4.10^{e}	0.886	0.282	14.465	162	12.120	12.566	14.664	2005706_{0}	-21.650	1.036	11.143	0.30
141	IC 4516	223.6166	16.3704	0.0456_{c}	0.0453_{1}	——	0.089	0.415	13.917	9	11.995	12.399	14.506	2365986_{1}	-22.459	0.988	11.378	1.45
142	ABELL 1991	223.6309	18.6420	0.0586_{c}	0.0592_{1}	5.40	0.804	0.090	14.456	42	11.961	12.372	14.479	2290443_{1}	-22.632	0.971	11.408	0.03
143	ABELL 2009	225.0850	21.3620	0.1530_{a}	0.1530_{2}	7.80	5.367	0.100	14.900	8427	11.799	12.355	14.466	3000021_{1}	-22.980	1.087	11.744	0.50
144	ABELL 2034	227.5489	33.5147	0.1130_{c}	0.1130_{2}	7.10^{e}	3.686	0.064	14.818	367	11.953	12.455	14.561	3000022_{1}	-22.839	1.049	11.656	1.69
145	ABELL 2029	227.7290	5.7200	0.0766_{a}	0.0766_{2}	7.80	8.391	0.260	15.030	12	12.242	12.666	14.772	3000023_{1}	-23.390	0.924	11.755	1.51
146	ABELL 2036	227.7761	18.0437	0.1161_{c}	0.1158_{1}	4.10^{e}	0.862	0.171	14.458	1353	11.629	12.085	14.230	2292145_{1}	-22.407	1.010	11.365	0.97
147	ABELL 2033	227.8480	6.3190	0.0817_{a}	0.0810_{1}	4.70^{e}	1.390	0.100	14.586	243	11.695	12.147	14.282	1366833_{1}	-22.562	1.027	11.521	1.96
148	SDSS-C4-DR3 1355	227.8897	1.7642	0.0384_{d}	0.0396_{1}	——	0.090	0.585	13.922	145	11.466	11.849	14.000	269480_{1}	-21.625	0.953	10.992	0.44
149	ABELL 2046	228.1553	34.8601	0.1489_{c}	0.1489_{2}	——	0.792	0.176	14.429	4285	11.925	12.432	14.535	3000024_{1}	-23.109	1.051	11.757	0.13
150	1RXS J151247.3-012753	228.2127	-1.4798	0.1223_{d}	0.1216_{1}	——	1.403	0.185	14.577	1393	11.696	12.173	14.308	577757_{1}	-22.538	1.031	11.435	0.51
151	ABELL 2052	229.1834	7.0185	0.0353_{c}	0.0342_{1}	3.40	1.276	0.036	14.576	24	11.786	12.211	14.343	1338000_{1}	-22.185	0.964	11.252	0.22
152	ABELL 2055	229.6899	6.2312	0.1021_{c}	0.1021_{1}	6.10^{e}	2.197	0.097	14.693	223	11.923	12.351	14.464	1333999_{0}	-21.929	0.803	11.094	0.07

TABLE 1
CONTINUED

(1)	(2)	(3)	(4)	(5)	(6)	(7)	(8)	(9)	(10)	(11)	(12)	(13)	(14)	(15)	(16)	(17)	(18)	(19)
153	ABELL 2064	230.2271	48.6693	0.1076_c	0.0738_1	5.30^e	0.774	0.102	14.443	212	11.680	12.081	14.227	999416_1	-23.021	0.926	11.515	0.76
154	ABELL 2061	230.3210	30.6400	0.0777_a	0.0788_1	5.60^e	2.237	0.150	14.704	29	12.196	12.599	14.697	1323246_1	-22.668	0.988	11.514	2.06
155	MKW 03s	230.4583	7.7088	0.0442_c	0.0447_1	3.00	1.472	0.051	14.609	51	11.653	12.104	14.248	1302169_1	-21.255	1.075	11.140	3.34
156	ABELL 2065	230.6106	27.7095	0.0723_c	0.0723_2	8.40	2.593	0.055	14.742	18	12.121	12.525	14.627	1460249_1	-21.613	1.017	11.083	0.67
157	ABELL 2063	230.7724	8.6025	0.0355_c	0.0342_1	4.10	0.948	0.046	14.503	17	11.752	12.176	14.312	1260227_0	-21.662	0.962	11.179	0.40
158	ABELL 2067	230.7830	30.8450	0.0756_b	0.0735_1	3.10^e	0.444	0.070	14.306	194	11.748	12.154	14.289	1327738_0	-21.844	0.958	11.098	1.95
159	ABELL 2069	231.0410	29.9210	0.1145_a	0.1135_1	7.90^e	4.978	0.150	14.892	259	11.976	12.435	14.539	1318942_1	-22.200	1.085	11.389	2.02
160	ABELL 2073	231.4360	28.4280	0.1515_b	0.1502_2	5.60^e	2.158	0.070	14.676	2926	11.955	12.438	14.544	1454463_1	-22.633	1.060	11.524	2.84
161	ABELL 2072	231.4770	18.2360	0.1270_a	0.1277_1	5.20^e	1.821	0.070	14.640	1110	11.852	12.271	14.397	2016591_1	-22.605	0.975	11.400	1.46
162	ABELL 2107	234.9100	21.7890	0.0411_a	0.0411_2	4.20	0.583	0.130	14.381	21	11.776	12.201	14.335	3000026_1	-22.433	0.934	11.408	0.41
163	ABELL 2110	234.9530	30.7173	0.0980_c	0.0972_1	5.60^e	2.095	0.107	14.683	1190	11.440	11.906	14.058	1388342_1	-22.524	1.001	11.407	0.52
164	ABELL 2108	235.0380	17.8780	0.0916_a	0.0886_1	4.30^e	1.022	0.100	14.508	182	11.828	12.248	14.375	2020473_1	-22.076	0.951	11.163	2.80
165	ABELL 2124	236.2500	36.0660	0.0654_a	0.0660_1	3.70^e	0.747	0.120	14.436	61	11.869	12.293	14.414	1412327_1	-22.644	0.979	11.443	2.62
166	MaxBCG J239.42665+35.50827	239.4382	35.5040	0.1549_c	0.1589_1	5.70^e	2.045	0.165	14.660	7475	11.671	12.149	14.284	1405455_1	-22.541	1.014	11.447	0.74
167	ABELL 2142	239.5857	27.2269	0.0894_c	0.0908_1	11.00	11.786	0.030	15.111	20	12.279	12.726	14.849	1400535_1	-22.521	1.041	11.450	0.42
168	ABELL 2149	240.3990	53.9180	0.0675_b	0.0654_1	3.00^e	0.423	0.050	14.296	99	11.709	12.157	14.293	501846_1	-22.175	1.039	11.341	2.61
169	RXC J1601.3+5354	240.3474	53.9061	0.1068_c	0.1071_1	——	1.306	0.079	14.563	811	11.602	12.006	14.161	250405_1	-22.743	0.970	11.453	2.38
170	ABELL 2147	240.5780	16.0200	0.0353_a	0.0353_1	4.40	1.500	0.220	14.616	2	12.174	12.577	14.677	2020680_0	-22.131	0.919	11.149	2.76
171	ABELL 2148	240.7590	25.4040	0.0888_b	0.0895_1	3.70^e	0.785	0.050	14.443	636	11.548	12.001	14.157	1323725_1	-22.473	0.973	11.353	5.33
172	NSC J160433+174311	241.1489	17.7244	0.0370_c	0.0351_1	3.50^e	0.464	0.070	14.326	6	12.115	12.536	14.638	1972342_0	-21.727	0.957	11.071	0.17
173	AWM 4	241.2380	23.9460	0.0318_a	0.0326_2	3.70	0.243	0.080	14.168	148	11.226	11.720	13.861	3000027_1	-22.166	0.993	11.374	0.81
174	ABELL 2152	241.3840	16.4420	0.0370_b	0.0435_1	1.70^e	0.125	0.050	14.001	10	11.992	12.399	14.505	1994658_0	-21.751	0.964	11.066	0.83
175	ABELL 2151E	241.7180	17.7810	0.0321_a	0.0390_1	1.30^e	0.055	0.040	13.799	6	12.115	12.536	14.638	1983734_0	-21.456	0.986	10.965	3.46
176	ABELL 2169	243.5400	49.1530	0.0579_b	0.0600_1	2.40^e	0.262	0.060	14.179	1027	11.093	11.491	13.606	532523_1	-21.473	0.977	10.958	3.63
177	RXC J1615.5+1927	243.8947	19.4600	0.0308_c	0.0316_1	——	0.061	0.140	13.825	608	10.934	11.371	13.463	1942972_1	-21.135	0.990	10.854	0.18
178	MaxBCG J245.12969+29.89103	245.1322	29.8953	0.0972_c	0.0960_1	5.00^e	1.669	0.084	14.627	118	12.025	12.455	14.560	1216685_1	-22.170	1.003	11.292	0.30
179	ABELL 2187	246.0591	41.2383	0.1825_c	0.1832_1	6.50^e	2.494	0.129	14.702	6978	12.239	12.784	14.921	1011568_1	-23.229	1.027	11.707	0.33
180	RXC J1627.3+4240	246.8482	42.6784	0.0317_c	0.0314_1	——	0.062	0.101	13.830	381	10.815	11.246	13.296	537847_1	-21.642	0.968	11.018	0.42
181	RXC J1627.6+4055	246.9173	40.9197	0.0301_c	0.0317_1	——	0.076	0.109	13.881	4	12.106	12.508	14.612	564226_1	-22.155	1.063	11.329	0.50
182	ABELL 2199	247.1582	39.5487	0.0299_c	0.0267_1	4.70	1.570	0.026	14.629	5	11.958	12.357	14.468	1009286_1	-21.856	0.943	11.086	0.38
183	NSC J164322+213144	250.8337	21.5261	0.1535_c	0.1536_1	——	0.973	0.173	14.478	7532	11.782	12.261	14.389	1434860_1	-22.871	1.040	11.583	0.30
184	NSC J165252+400906	253.2318	40.1535	0.1492_c	0.1504_2	5.00^e	1.786	0.133	14.629	6300	11.582	12.054	14.205	260130_1	-22.443	1.011	11.375	0.60
185	RXC J1654.3+2334	253.5972	23.5699	0.0575_c	0.0570_1	——	0.190	0.135	14.101	322	11.287	11.692	13.831	1404809_1	-21.480	0.961	10.984	0.24
186	ABELL 2241B	254.9365	32.6135	0.1013_c	0.1013_2	4.30^e	1.169	0.099	14.538	949	11.598	12.041	14.194	1013809_1	-22.808	1.021	11.518	0.23
187	ABELL 2245	255.6330	33.5130	0.0843_b	0.0864_1	3.20^e	0.536	0.040	14.349	136	11.901	12.352	14.465	580244_1	-22.824	1.014	11.550	0.38
188	ABELL 2244	255.6786	34.0619	0.0953_c	0.0989_1	7.10	4.470	0.038	14.869	192	11.857	12.336	14.450	3000028_1	-22.630	0.901	11.416	0.15
189	ABELL 2249	257.4535	34.4406	0.0802_c	0.0809_2	5.60^e	1.883	0.061	14.661	208	11.729	12.161	14.296	583901_1	-22.160	1.012	11.288	1.10
190	ABELL 2255	258.1968	64.0614	0.0809_c	0.0734_1	7.30	2.593	0.042	14.741	178	11.749	12.167	14.303	236440_1	-22.596	0.960	11.381	4.61
191	NGC 6338 GROUP	258.8414	57.4074	0.0276_c	0.0273_1	2.40^e	0.250	0.154	14.176	72	11.396	11.825	13.976	199782_1	-22.058	0.996	11.226	0.35
192	ABELL 2257	259.4731	32.5860	0.1054_c	0.1086_1	——	1.094	0.126	14.519	1758	11.521	12.005	14.160	519321_1	-22.678	1.016	11.497	0.75
193	RBS 1636	259.5410	56.6656	0.1138_c	0.1136_1	5.00^e	1.772	0.085	14.637	6235	11.370	11.783	13.930	202925_1	-22.568	0.870	11.309	0.52
194	ABELL 2259	260.0370	27.6702	0.1640_c	0.1640_2	7.10^e	3.600	0.086	14.798	3963	12.076	12.588	14.690	3000029_1	-23.240	1.085	11.845	0.21
195	SDSS-C4 3072	260.0386	26.6272	0.1644_c	0.1601_1	10.20^e	6.921	0.064	14.961	1039	12.469	12.880	15.052	566931_1	-23.224	0.907	11.593	0.22
196	MaxBCG J321.29330-06.96355	321.3016	-6.9655	0.1153_d	0.1153_2	——	1.107	0.367	14.521	1954	11.497	12.074	14.221	3000030_1	-22.493	1.134	11.609	0.51
197	ABELL 2396	328.9198	12.5336	0.1920_c	0.1930_1	6.90^e	3.392	0.168	14.775	6426	12.300	12.822	14.984	350905_1	-23.641	1.027	11.872	0.62
198	ABELL 2399	329.3573	-7.7946	0.0579_d	0.0580_1	——	0.480	0.190	14.329	27	11.987	12.386	14.490	313506_0	-21.801	0.950	11.052	0.92
199	ABELL 2428	334.0645	-9.3399	0.0825_d	0.0846_1	——	1.674	0.101	14.631	209	11.793	12.270	14.397	732935_1	-22.567	1.017	11.521	0.40
200	ABELL 2561	348.4990	14.7440	0.1627_b	0.1625_1	5.30^e	1.918	0.050	14.643	1569	12.284	12.703	14.810	351366_0	-21.863	1.044	11.200	0.51
201	RXC J2321.8+1505	350.4671	15.0430	0.1500_c	0.1490_1	——	1.243	0.150	14.540	15567	11.382	11.840	13.990	719109_1	-22.525	1.002	11.398	2.73
202	ABELL 2593	351.0840	14.6510	0.0428_a	0.0417_1	3.10	0.590	0.120	14.384	8	12.014	12.444	14.550	717807_1	-22.322	0.981	11.314	0.23
203	ABELL 2670	358.5557	-10.4129	0.0765_d	0.0776_1	——	1.511	0.121	14.607	23	12.194	12.618	14.716	356435_1	-22.751	1.007	11.533	0.38

Notes on individual entries in Table 1:
WBL 032 Two massive galaxies **VV 377 NED01** and **VV 382 NED01** appear to be equally dominant, separated in projection by 4.2 arcmin. C99 regards the latter as the central galaxy. However, Chandra image shows that the former galaxy is at the first maximum point (FMP) of the X-ray intensity of emission. We take the former as the central which is not the MMG.
ABELL 0168 Both XMM-Newton and Chandra images show **ABELL 0168(N) (i.e. galaxy UGC 00797)** takes the place of **ABELL 0168(S)** to be the X-ray FMP. C99 points that the X-ray image of the cluster is broad with no tight core, and the brightest cluster galaxy is clearly the central.
RXC J0736.4+3925 contains a non-MMG with QSO-like spectrum nearby the X-ray centroid (≤ 1 arcmin). And the SDSS image shows the non-MMG seem to be an AGN or a galaxy overlapped by a star. In stead, we adopt **2MASX J07363812+3924525** as the central galaxy of this cluster, leading an offset 3.36 arcmin.
ABELL 0763 As discussed in C99, the same galaxy **SDSS J091235.18+160000.6** is used as the central.
ABELL 0757 The X-ray image of the cluster has 2 maxima. The MMG (central) is at the FMP i.e. (138.2586,47.7059)–(in format R.A.,Dec. Hereafter the format like this stands for a source's position in J2000d; see also Table 6 in Böhringer et al. 2000)
SDSS J100031.02+440843.3 or **RBS 0819** Both XMM-Newton and Chandra confirm the non-MMG **SDSS J100031.00+440843.2** is the central of the cluster.
RX J1053.7+5450, SDSS-C4-DR3 3043 and **RXC J1121.7+0249** These X-ray sources are all very extended and unfortunately no associated Chandra or XMM-Newton images. Centrals are the MMGs.
ABELL 1314 The central locates exactly at the X-ray centroid in Chandra and XMM-Newton images, and is the same one adopted by C99 (173.7041,49.0776).
ABELL 1361 The X-ray image of the cluster has 2 maxima. Following C99, the central is at (175.9146,46.3561), also the FMP, and confirmed by Chandra image.
ABELL 1366, RXC J1229.9+1147, RBS 1198, ABELL 1612, RXC J1416.5+3045 and **ABELL 1925** are all very extended sources in the RASS image. The X-ray maxima for the first 3 sources are determined by the Chandra and/or XMM-Newton high resolution images at (176.1535,67.4058),(187.5486,11.7444) and (194.8982,27.9596) respectively. Moreover, the centrals of the enrolled sources **RXC J1229.9+1147** and **RXC RBS 1198** in C99 locate at the very positions of the their (above) X-ray maxima. In the absence of higher resolution X-ray images, we choose the MMGs as centrals for the last 3 clusters.
ABELL 1367 is a very well-studied merging cluster. Member galaxies around the X-ray centroid are much less massive (at least one order of magnitude) than the BCG (NGC 3862, which is associated with the strong radio source 3C264, see C99). Although the BCG of this cluster is significantly offset ~ 666 kpc (11.61 arcmin $\ll r_{500c} = 33.61$ arcmin) from the center of the highly extended X-ray emission, we take it as the central galaxy of this X-ray cluster.
ABELL 1902, ABELL 1930 and **ABELL 2033** are sources cataloged by C99. We use the galaxies provided by C99 as their centrals (also the MMGs), and the latter 2 cross-identifications are confirmed by ROSAT HRI and PSPC with a little offset ≤ 0.5 arcmin.
ABELL 2061 has a broad X-ray image. C99 suggests that the cluster is consist of 2 (Northern and Southern) components. And Chandra image shows **ABELL 2061(N)** (230.3354,30.6711) is the X-ray FMP, and also the location of its central.
MKW 03s Images from 3 instruments (ROSAT/PSPC, XMM-Newton and Chandra) show that the X-ray FMP is at (230.4662,7.7089) where also lies the MMG of the cluster (see also C99).
ABELL 2067 The X-ray image from ROSAT/PSPC (230.7815,30.8718) supports the non-MMG **2MASX J15230842+3052387** as the cluster central.
ABELL 2069 Following C99 we choose **2MASX J15240741+2953203** (the northern component of a pair in contact) as the cluster central, which is also confirmed by a check according to the PSPC and Chandra images.
ABELL 2073 and **ABELL 2169** Their RASS images are all very extended. Thus the MMGs are their centrals.
ABELL 2018 The cluster central is **SDSS J154019.03+175123.3** (see C99).
ABELL 2124 Chandra image shows the X-ray FMP is at (236.2462,36.1097), the right position of the central galaxy **UGC 10012** (see C99).
ABELL 2149 and **RXC J1601.3+5354** are very close in projection but with very different redshifts (multiple redshift clustering in line-of-sight). And they have the same one X-ray image (very extended) in RASS. Here we are not sure whether the foreground and background contamination on X-ray flux is taken into account in their reference papers.
ABELL 2147 C99 suggests **UGC 10143** (240.5708,15.9750) as the optical counterpart of the X-ray centroid of the cluster, which is supported by the images from ROSAT/PSPC, XMM-Newton and Chandra.
ABELL 2148 and **ABELL 2151E** For each of them, the optical identification of the point-like object at the X-ray centroid (ROSAT/PSPC) is of a star. In this case we use the galaxies corresponding to the second maximum points of X-ray intensity as the centrals.
ABELL 2255 Images from XMM-Newton and Chandra show that the X-ray FMP is at (258.1471,64.0624) where the nearest galaxy is **ZwCl 1710.4+6401 A**, also the MMG.
RXC J2321.8+1505 The X-ray FMP on RASS images is at (350.4535,15.0849), very close to the MMG **2MASX J23214705+1504594**.
AWM 4 Instead of using its unreliable X-ray luminosity (suffering from very large uncertainty 0.979) from Böhringer et al. (2000), we extract the record from Ebeling et al. (1998).

Majumdar, S., & Mohr, J. J. 2004, ApJ, 613, 41
Mantz, A., Allen, S. W., Ebeling, H., Rapetti, D., & Drlica-Wagner, A. 2010a, MNRAS, 406, 1773
Milosavljević, M., Miller, C. J., Furlanetto, S. R., & Cooray, A. 2006, ApJ, 637, L9
Mo, H. J., & White, S. D. M. 1996, MNRAS, 282, 347
More, S., van den Bosch, F. C., Cacciato, M., Mo, H. J., Yang, X., & Li, R. 2009, MNRAS, 392, 801
Mulchaey, J. S., Davis, D. S., Mushotzky, R. F., & Burstein, D. 2003, ApJS, 145, 39
Navarro, J. F., Frenk, C. S., & White, S. D. M. 1997, ApJ, 490, 493
Peacock, J. A., & West, M. G. 1992, MNRAS, 259, 494
Piffaretti, R., Arnaud, M., Pratt, G.W., Pointecouteau, E., Melin, J.B., 2010, A&A in press (arXiv:1007.1916)
Ponman T. J., Allan D. J., Jones L. R., Merrifield M., McHardy I. M., Lehto H. J., Luppino G. A., 1994, Nature, 369, 462
Popesso, P., Böhringer, H., Brinkmann, J., Voges, W., & York, D. G. 2004, A&A, 423, 449
Popesso, P., Biviano, A., Böhringer, H., & Romaniello, M. 2007, A&A, 461, 397
Pratt, G. W., Croston, J. H., Arnaud, M., & Böhringer, H., 2009, A&A, 498, 361
Reiprich, T. H., & Böhringer, H., 2002, ApJ, 567, 716
Rozo, E., et al. 2009a, ApJ, 699, 768
Rozo, E., et al. 2009b, ApJ, 703, 601
Rykoff, E. S., et al. 2008a, ApJ, 675, 1106
Rykoff, E. S., et al. 2008b, MNRAS, 387, L28
Sheth, R. K., Mo, H. J., & Tormen, G. 2001, MNRAS, 323, 1
Skibba, R. A., van den Bosch, F. C., Yang, X., More, S., Mo, H., & Fontanot, F. 2011, MNRAS, 410, 417
Stanek, R., Evrard, A. E., Böhringer, H., Schuecker, P., Nord, B., 2006, ApJ, 648, 956
Tinker, J., Kravtsov, A. V., Klypin, A., Abazajian, K., Warren, M., Yepes, G., Gottlöber, S., & Holz, D. E. 2008, ApJ, 688, 709
van den Bosch, F. C., Yang, X., Mo, H. J., & Norberg, P. 2005, MNRAS, 356, 1233
van den Bosch, F. C., Yang, X., Mo, H. J., Weinmann, S. M., Maccio, A., More, S., Cacciato, M., Skibba, R., & Kang, X., 2007, MNRAS, 376, 841
Vikhlinin et al., 2009a, ApJ, 692, 1033
Vikhlinin, A., et al. 2009b, ApJ, 692, 1060
Voges, W., et al. 1999, A&A, 349, 389
Watson, M.G. et al., 2009, A&A 493, 339
Yan, R., Madgwick, D. S., & White, M. 2003, ApJ, 598, 848
Yang X., Mo H.J., van den Bosch F.C., 2003, MNRAS, 339, 1057
Yang X., Mo H.J., van den Bosch F.C., Jing Y.P., 2005a, MNRAS, 356, 1293

Yang, X., Mo, H. J., van den Bosch, F. C., Weinmann, S. M., Li, C., & Jing, Y. P. 2005b, MNRAS, 362, 711
Yang X., Mo H.J., van den Bosch F.C., Pasquali A., Li C., Barden M., 2007, ApJ, 671, 153
Yang X., Mo H.J., van den Bosch F.C., 2008, ApJ, 676, 248
Yang X., Mo H. J., van den Bosch F. C., 2009, ApJ, 695, 900
Yang, X., Mo, H. J., van den Bosch, F. C., Zhang, Y., & Han, J. 2011, arXiv:1110.1420
Yee, H. K. C., & Ellingson, E. 2003, ApJ, 585, 215
Zehavi, I., et al. 2002 ApJ, 571, 172
Zhang, Y.-Y., Andernach, H., Caretta, C. A., Reiprich, T. H., Böhringer, H., Puchwein, E., Sijacki, D., & Girardi, M. 2011, A&A, 526, A105
Zhao, D. H., Jing, Y. P., Mo, H. J., & Boerner, G. 2009, ApJ, 707, 354
Zwicky F., Herzog E., Wild P., Karpowicz M., Kowal C.T., 1961-68, Catalogue of Galaxies and Cluster Galaxies, Vols 1-6